國 立 交 通 大 學

電機學院微電子奈米科技產業研發碩士班

碩 士 論 文

利用氧化提昇矽鍺奈米線生物感測器之靈敏度

The Enhancement of the Sensitivity for SiGe
Nanowire Bio-sensor by Oxidation

研 究 生：趙文全

指導教授：汪大暉　教授

中 華 民 國 九 十 七 年 二 月

利用氧化提昇矽鍺奈米線生物感測器之靈敏度

The Enhancement of the Sensitivity for SiGe Nanowire Bio-sensor by Oxidation

研 究 生：趙文全　　　　　Student：Wen-Chuan Chao

指導教授：汪大暉　　　　　Advisor：Tahui Wang

國 立 交 通 大 學

電機學院微電子奈米科技產業研發碩士班

碩 士 論 文

A Thesis
Submitted to College of Electrical and Computer Engineering
National Chiao Tung University
in partial Fulfillment of the Requirements
for the Degree of
Master
in

Industrial Technology R & D Master Program on
Microelectronics and Nano Sciences

February 2008

Hsinchu, Taiwan, Republic of China

中華民國九十七年二月

利用氧化提昇矽鍺奈米線生物感測器之靈敏度

學生: 趙文全　　　　　　　　　　指導教授: 汪大暉 博士

國立交通大學電機學院產業研發碩士班

摘　　要

　　矽基材之奈米線在近年來已被廣範的研究。然而,就敏感度而言,矽鍺奈米線比矽基材之奈米線更有潛力,這是因為當同樣數量的待測物質鍵結於表面時,矽鍺奈米線有較大的電流變化。此外,我們發現敏感度會隨著鍺濃度增加而增加(7%~30%)。

　　但是,製作高濃度之矽鍺奈米線有其困難度。因此,我們利用氧化的過程,使鍺由氧化層中析出,並獲得高濃度的矽鍺奈米線。經過900℃、2 分鐘氧化後,我們可以發現低濃度(7%、11%、20%)的矽鍺奈米線,其靈敏度均有提升。經過 950℃、2 分鐘氧化後,我們發現鍺濃度 7%的奈米線的靈敏度繼續提昇,但鍺濃度 11%的奈米線的靈敏度並沒有繼續增加,這可能是在氧化的過程中產生過多的缺陷所造成。
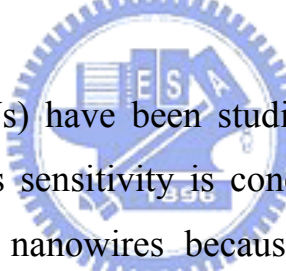
The Enhancement of the Sensitivity for SiGe Nanowire Bio-sensor by Oxidation

Student: Wen-chuan Chao   Advisors: Dr. Tahui Wang

Industrial Technology R & D Master Program of
Electrical and Computer Engineering College
National Chiao Tung University

ABSTRACT

Si nanowires (SiNWs) have been studied for Bio-sensor in recent years. However, as far as sensitivity is concerned, SiGe nanowires are more promising than Si nanowires because of SiGe nanowires have higher change in drive current when the same chemical species bonding to surface of nanowire. In addition, we have reported the sensitivity increase with Ge concentration (7%~30%).

But it is difficult to fabricate higher Ge concentration nanowire. Therefore, we utilize oxidation process to enhance Ge concentration in SiGe nanowire because Ge is rejected from the oxide during oxidation process. We found that the sensitivity of lower Ge concentration (7%~20%) nanowires were enhanced by oxidation process after the oxidation of 2min at 900°C. After the oxidation of 2min at 950°C, we observed that the sensitivity of $Si_{0.93}Ge_{0.07}$ nanowires were improved but the sensitivity of $Si_{0.89}Ge_{0.11}$ nanowires not increased. The reason maybe higher defect was formed during this oxidation process.

Contents

Figure Captions

Table Captions

Chapter 1

Introduction

1.1 The application of nanowire sensors

Nanowires (NWs) have been attracting considerable attention in recent years. The application of nanowires has been the topic of significant recent research [1~5]. In fact, the downscaling of material dimension does not only imply an increase in device packing density and a decrease in power consumption, but also it renders superior sensitivity. Semiconductor nanowires are particularly appealing for sensing applications because of large surface -to-volume ratio [6~9].

Nanowire sensors were fabricated by various material, such as silicon nanowire sensors [10~11], metal oxide nanowire sensor [12~15], polymer nanowire sensesors [16~17], and metal nanowire sensors [18~19]. As far as detected source are concerned, nanowire sensors have been demonstrated for detection of various gases, pH inaqueous media, antibody binding, virus, single cancer markers, and DNA hybridization, and so forth. All application of nanowire sensors are listed in table 1-1.

1.1.1 The application of silicon nanowire sensors

Silicon nanowires (SiNWs) are particularly appealing for sensing applications, since the silicon oxide can effectively passivate surface dangling bonds, and at the same time can be chemically modified through the well known silanol chemistry to provide surface functionalization and, therefore, selectivity for particular analytes.

pH sensors.　In previous report [1], silicon nanowire solid state FET, whose conductance is modulated by an applied gate, is transformed

into a nanosensor by modifying the silicon oxide surface with 3-aminopropyltriethoxysilane (APTES) to provide a surface that can undergo protonation and deprotonation, where changes in surface charge can chemically gate the silicon nanowire ,as shown in Figure 1-1. The conductance versus pH show that this pH dependence is linear over the pH 2 to 9 range and thus suggest that modified silicon nanowires could function as nanoscale pH sensors, as shown in figure 1-2.

Biomolecular sensors. Biotin-modified Silicon nanowires were used to detect streptavidin, as shown in Figure 1-3. The conductance of biotin-modified silicon nanowires increase rapidly to a constant value upon addition of a 250nM and that this conductance value is maintained after the addition of pure buffer solution, as shown in Figure 1-4.

Monoclonal antibiotin sensors. Binding of biotin-monoclonal antibiotin (m-antibiotin) is reversible interaction. Plot of conductance versus time for a biotin-modified silicon nanowires exhibit a well-defined drop after addition of m-antibiotin solution followed by an increase in the conductance to about the original value upon addition of pure buffer solution, as shown in Figure 1-5.

DNA sensors. Silicon nanowires have been demonstrated to detect DNA molecules [10]. Nanowires were exposed to the vapor of 3-mercaptopropyltrimethoxysilane (MPTMS) in argon for 4 h, followed by rinsing with absolute ethyl alcohol, and blown-dry with nitrogen. The immobilization of ss-DNA probes was achieved by exposing the MPTMS-covered samples to a 5 μM solution of the oligonucletides modified with acrylic phosphoramidite funcyional groups at the 5′ position for 12 h. The hybridization of the DNA probes on the surface

with the complimentary DNA target further reduced the surface photovoltage signal by an additional ~3mV, as shown in Figure 1-6. When the target DNA attached to its complementary DNA on the SiNW surface, the increase of negative charges introduced by the DNA enhanced the carrier concentrations in p-type SiNWs, resulting in the observed changes of the conductance, as shown in Figure 1-7.

Virus sensors. A two-step procedure was used to covalently link antibody receptors to the surface of the silicon nanowire devices [11]. First, the devices were reacted with a 1% ethanol solution of 3-(trimethoxysilyl)propyl aldehyde for 30 min, washed with ethanol, and heat at 120°C for 15min. Second, mAb receptors, anti-hemagglutinin for influenza A and anti-adenovirus group Ⅲ, were coupled to the aldehyde-terminated nanowire surface by reaction of 10-100 μg/ml antibody in a pH 8, 10-mM phosphate buffer solution containing 4mM sodium cyanoborohydride. Figure 1-8 show that as a virus particle diffuses near a nanowire device the conductance remains at the baseline value, and only after binding at the nanowire surface dose the conductance drop, where the conductance change, ~18 nS. When the virus unbinds and diffuses from the nanowire surface the conductance returns to the baseline value.

1.1.2 The application of metal oxide nanowire sensors

The fundamental sensing mechanism of metal oxide base gas sensors relie on a change in electrical conductivity due to the interaction process between the surface complexes and the gas molecules to be

detected. Metal oxide nanowire were synthesized by thermal evaporation of oxide powders under controlled conditions without the presence of a catalyst. Ultralong nanowires have been successfully synthesized for ZnO, SnO_2, In_2O_3 and WO_3 by simply evaporating the desired commercial metal oxide powders at high temperature [12~15].

Gas sensors have been fabricated using the SnO_2 nanowires [13]. The esponses of the sensors have been characterized for gaseous polluting species like CO and NO_2 for environmental applications, as well as for ethanol for breath analyzers and food control applications. The response of the current flowing through the SnO_2 nanowires when two square concentration pulses of CO (250 and 500 ppm) are fed into the test chamber, at a working temperature of 400°C and 30% RH. The electric current increases for about 60% and 100% with the introduction of 250 and 500 ppm CO, respectively, as shown in Figure 1-9.
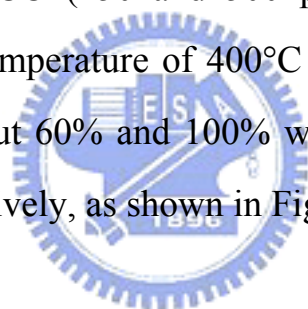
1.1.3 The application of polymeric nanowire sensors

Conducting polymers have attractive features such as mechanical flexibility, ease of processing, and modifiable electrical conductivity. Polymeric nanowire sensors were been studied in some literature [16~17].

Polyaniline/poly-(ethylene oxide) (PANI/PEO) nanowire sensors that can detect NH_3 gas at concentrations as low as 0.5 ppm with rapid response and recovery time [16]. The measured current versus time curves, which reflect the gas-concentration dependence of the temporal conductance behavior, as shown in Figure 1-10.

1.1.4 The application of metal nanowire sensors

Pd nanowires have been studied to detect hydrogen gas due to safety reasons [18]. The sensor based on resistance change of Pd nanowires upon hydrogen incorporation. The change of resistance was attributed to swell of volume of Pd nanowire in the presence of hydrogen gas [19]. The measured electrical resistance versus time curves exhibited sharp decreases upon hydrogen injections. The electrical resistance change is dependent on hydrogen concentration, as shown in Figure 1-11.

1.2 Fabrication of nanowire

Nanowires are essentially 1D structures with unique optical and electrical properties. Therefore, nanowires have attracted increasing interest for device use in logic gates [20], address decoders [21], memory components [22], light emitting diodes [23], photodetectors[24], lasers[25], and chemical sensors[1]. Various approaches for growing nanowires, including (1) lithography with photons in UV, DUV, EUV and X-ray spectrum; (2) machining using AFM, STM, NSOM; (3) nanoimprint lithography; (4) spacer formation; (5) vapor state synthesis; (6) vapor-liquid-solid growth approach; (7) electrochemical deposition.

1.2.1 Lithography with photons

In photon and particle-based lithography, by using nonlinear resists, near-field phase shifting or topographically directed technology, it has been possible to achieve sub-50nm feature. For example, EBL has demonstrated the ability to achieve 20nm width nanowires with 60nm

height. Height is often limited by the lift-off process. Extreme ultraviolet light (EUV) lithography has generated 38nm patterns [26].

1.2.2 Machining using AFM, STM, NSOM

In 1990, J. A . Dagata *et al*. proposed the tip-induced anodic surface oxidation by using scanning probe lithography (SPL) to define nano-patterns on the semiconductor surface, as shown in Figure 1-12. AFM, STM and NSOM and the like are called SPM. Its operation mechanism is in an environment humidity control when approximately 50%, the sample surface attaches a water thin film, when the probe contacts this water thin film, take the probe as negative electrode, the sample surface is the positive electrode, gives a negative bias to probe, the water molecule can start to ionization, and produces the partial region oxide compound with the probe under- neath sample surface. The probe produces the electric field can along with the distance of sample surface to attenuation, the oxidation stops immediately when the electric-field intensity is smaller than 10^9 V/m. [27] The oxide compound growth speed with executes gives the probe bias to have the enormous relations. In process by way of program configure, but fine holds controls scans the probe the displacement, carries on oxide compound of the specific line to grow, then achieves the micro region design forming the goal, this is scanning probe lithography technique to apply to the lithography at the beginning of shape.

1.2.3 Nanoimprint lithography (NIL)

Nanoimprint lithography is a novel method of fabrication nanometer scale patterns. In previous report [28], the single crystalline Si nanowire structures are fabricated as a mold for producing high surface area Pt wire. PMMA are spined on substrate and are used as imprint resist. The process flow for nanoimprint patterning is shown in Figure 1-13

1.2.4 Spacer formation

Controlled deposition and size reduction, which involves deposition on cleaved edges, or oxidation, followed by anisotropic etching forming spacers, as shown in Figure 1-14. This process provides a density increase as well as size reduction. It can be used to pattern silicon fins for double-gate MOSFETs.[29]
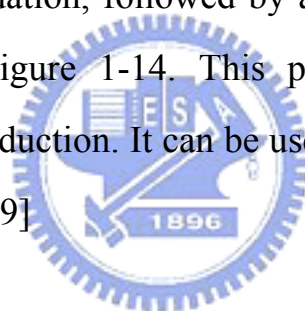
1.2.5 Vapor state synthesis

Vapor state synthesis of single-crystalline freestanding Ag nanowire have been repoted [30]. Their synthetic method is unique in that it uses only a single reactant, Ag_2O, without using any templates or catalysts. In a typical synthesis, Ag_2O powder was placed in an alumina boat in the middle of horizontal quartz tube furnace. The NWs were grown at a few centimeters downstream from the precursor on a Si substrate. At high temperature (T = 900°C-1000°C), the precursor vapor was carried downstream by the flow of Ar to a lower temperature zone (T = 500°C), where Ag NWs were grown.

1.2.6 Vapor-liquid-solid (VLS) growth approach

Vapor state synthesis grown nanowires lack a diameter-control mechanism. Diameter of nanowires can be controlled by the catalyst nanoparticle size. Zhou's group reported an efficient route for the synthesis of single-crystalline In_2O_3 nanowires via the VLS mechanism, where the In vapor was generated by laser ablation of an indium-containing target. Excellent diameter control was achieved by using monodispersed gold clusters as the catalyst [31].

1.2.7 Electrochemical deposition

Anodized aluminum oxide (AAO) is a poriferous material. The advantages of AAO film including the possibility to fabricate larger areas, the ability to produce a greater range of pore sizes, and the ability to grow into the pores at higher temperature [32]. The ordered nanowires and nanoparticles were electrodeposition into the nanopores of AAO film. After removing AAO template, the free-standing nanowires were formed.

1.3 Ge enhance the sensitivity of SiGe nanowire

SiGe-channel transistor have larger drain current at the same V_{GS}-V_{TH}, as show in Figure 1-15 [33]. This result point out SiGe nanowires may be have higher change in electrical property at the same chemical species bonding to surface of nanowires.

Sensitivity is a important parameter of nanowire sensors. To achieve higher sensitivity of nanowire sensors, we have proposed SiGe nanowire sensors. In our previous report, we have successfully fabricated the

nanowire with different Ge concentration respectively and demonstrated that the sensitivity was improved by using higher Ge concentration (7% ~ 30%) nanowire. But our experiment found the higher Ge concentration (40%) has not increased the sensitivity; the reason maybe the higher defect appears at the surface as higher Ge concentration [34], as show in Figure 1-16.

1.4 Ge condensation process in SiGe film

The oxidation of SiGe thin films has been demonstrated at several laboratories [35~38]. In all cases reported so far, it is shown that Si is preferentially oxidized and only one Ge-rich layer is formed at the oxide/substrate interface for SiGe with a Ge concentration below 50%. On the other hand, there are two oxide layers formed after oxidation for SiGe with Ge concentration above 50%.
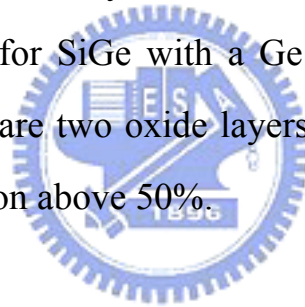
1.4.1 Oxidation mechanism of SiGe

According to the theory binary alloy oxidation [39~40], the oxide growth will depend on the alloy composition. For the case of the SiGe alloy, Si is more reactive than Ge. The reason is the large difference between the heat of formation of SiO_2 (-204 kcal/mol) and GeO_2 (-119 kcal/mol). For SiGe with low Ge concentration (**< 50%**), only silicon is oxidized initially. Ge is completed rejected from the oxide and piles up at the oxide/substrate interface. On the other hand, oxygen concentration at the oxidation front decreases with the oxide thickness increases. Then, the decreasing oxygen concentration at the oxidation front counteracts the

effect of increasing Ge concentration in the Ge-rich SiGe layer so that Ge is not oxidized during the entire oxidation process.

For SiGe with high Ge concentration (> 50%), Si and Ge will be oxidized during the oxidation process. During the oxidation process, the oxygen concentration decrease with increasing oxide thickness, leading to a decrease of the oxidation rate. Therefore, the Si is enough to react with oxygen to form a pure SiO_2 layer. During the formation of the mixed oxide, no pileup of Ge at the interface is expected, since Ge is being oxidized. When a pure SiO_2 layer is being formed though, Ge will pile up at SiO_2/substrate interface.

1.4.2 Oxidation behavior of SiGe

The oxidation behavior of SiGe films has been studied to a great extent [41~43]. Ge is completed rejected from the oxide and piles up at the oxide/substrate interface after oxidation process. The total amount of Ge atoms in the SiGe layer is conserved. This is because Ge atoms is blocked by the BOX layer and thermal oxide layer due to the much lower diffusion coefficient in SiO_2. A Ge-on-insulator (GOI) was fabricated by Ge condensation technique in previous literature [44]. In addition, as the thickness of SiGe layer is smaller than diffusion length of the Ge atoms, the SiGe layer will become uniform, as show in Figure 1-17. During the oxidation process, defects will generate in SiGe layer. If Ge fraction in the SiGe layer exceed critical enrichment value, defect will increase rapidly [45~46].

In order to improve the hole mobility of CMOS, the SiGe-on-Insulator pMOSFET has been reported [47]. They utilized Ge

condensation technique to fabricate SiGe channel with various Ge concentration. The mobility enhancement factor at E_{eff} of o.5MV/cm as a function of Ge concentration, as shown in Figure 1-18.

1.5 Motivation

We have been demonstrated the enhancement of sensitivity of SiGe nanowire with Ge concentration. But, it is difficult to obtain SiGe layer with high Ge concentration because the large lattice mismatch between the SOI and SiGe layer. Ge-condensation technique is a method to enhance Ge concentration in SiGe layer without generating defect. Therefore, we utilize oxidation process to ehance Ge concentration in SiGe nanowire and the surface-to-volume ratio of SiGe nanowires will become higher.

Chapter 2

Experiment

The spacer formation [31] is an easy process for nanowire-fabrication with the advantages of high-yield and low-cost. The method only using the combination of the conventional lithography and process technology was demonstrated without complex processes such as EBL, SPL and VLS etc. We have successfully fabricated the SiGe nanowires by this method. To enhance sensitivity of SiGe-nanowire with low Ge concentration, Ge-condensation technique was utilized to obtain higher Ge concentration in SiGe nanowire after oxidation. And SiGe nanowire has higher surface-to-volume ratio, less defect and higher conductance which will discuss later.
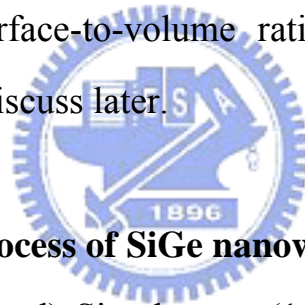
2.1 Detail fabrication process of SiGe nanowire

A p-type (Boron doped) Si substrate (100) was used in this study. The resistivity of the silicon substrate is about 1~10 Ω-cm. Samples were prepared by follow process:

1. After Standard RCA clean, wet oxidation for 6 hours at 980°C to grow the bottom oxide by *ASM/LB45 furnance system*. The thickness of oxide is 5000Å which was shown in Figure 2-1.

2. Mask #1: Define the active area. We utilize *TEL CLEAN TRACK MK-8* and *G-line lithography system* to transfer pattern on bottom oxide. Then, we etch a height step to form a SiGe spacer by *TEL5000 R.I.E. system*. The height of step is about 3000 Å. The structure was shown in Figure 2-2.

3. Following Standard RCA clean, we deposited 150Å α-Si layer on bottom oxide by *ASM/LB45 furnance system*. The growth condition of 150Å α-Si layer was 650°C for ~2 hours. The process increases adhesion between SiGe film and SiO_2 layer shown in Figure 2-3.

4. After Standard RCA clean, we deposited SiGe film by ultra-high -vaccum chemical vapor deposition − *ANELAVA SiGe UHV-CVD*. The condition of the SiGe film was epitaxially grown at 665°C. The structure was shown in Figure 2-4.

5. Mask #2: Defined the S/D region and nanwires. We etched the α-Si and SiGe film by *TCP poly etcher* − *TCP9400 SE*. Only the S/D and SiGe nanowires will be stayed. The structure was shown in Figure 2-5.

6. Mask #3: To avoid parallel SiGe nanowires short-circuit each other, we used *TCP poly etcher* to etch over two side spacer. The structure was shown in Figure 2-6.

7. Oxidation in various conditions such as different temperature and time.

8. The condition of ion implantation was E =15keV in energy and D =5×10^{15} P^+ ions/cm^2 in dose.

9. After ion implantation, the surface oxide layer was removed by DHF (H_2O:HF=50:1).

10. Aluminum layer with 5000 Å thick was coated on the wafer by Thermal Coater.

11. Mask #4: Defined aluminum contact. Aluminum contact pad were defined by wet etching (HNO_3:CH_3COOH:H_3PO_4:H_2O=2:9:50:10). The structure was shown in Figure 2-7.

12. Al sintering at 400℃ in N_2 ambient for 30 minutes.

2.2 The process of measurement

HP4156A is an electronic instrument for measuring and analyzing characteristics of semiconductor devices. I_D-V_D characteristics of our experiment were measure by HP4156A.

2.2.1 The measurement of Bio-sensor

1. The measure conditions were set V_D= -10V to 10V in 0.2 step and V_G= -15V, 0V, 15V respectively.

2. The SiGe nanowire was modified by 3-aminopropyltrimethoxysilane (APTMS) which could connect to the bio-linker BS3.

3. Drip bis(sulfosuccinimidyl) suberate sodium (BS3) solution as linker which could connect to the antibody IgG molecules.

4. The antibody IgG molecules were applied to link after BS3.

5. I_D-V_D curve was measured by HP4156A.
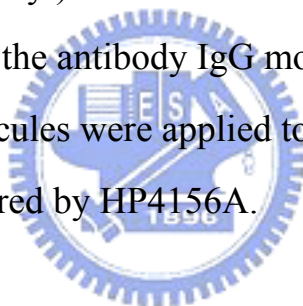
Chapter 3

Results & Discussion

To obtain the dimension of SiGe nanowire, the cross-section view of SiGe nanowire was observed by Scanning Electron Microscopy (SEM). In addition, we utilized HP4156A to measure the I_D-V_D characteristics in our experiment when different molecular was adhered. All result will be discussed in this chapter.

3.1 Dimension of SiGe nanowires

The dimension of SiGe nanowire was controlled by the deposition for the width and the step of oxide for the height. In order to etch the SiGe film clearly, we added the 20% over-etching at the step of dry etching. The Scanning Electron Microscopy (SEM) was utilized to observe the cross-section view of SiGe nanowire. The *JOEL JSM 6500-F-TFSEM* was the equipment which we used to measure the diameters of the nanowires. Figure 3-1~3-5 show the cross-section view SEM image of different Ge concentration nanowires before oxidation process. The area and surface-to-volume ratio were summarized in the Table 3-1.

After the oxidation of 2 min at 900℃, the cross-section view SEM image of different Ge concentration nanowires were shown in Figure 3-6~3-10. The area and surface-to-volume ratio were also summarized in the Table 3-2. The increment of the surface-to-volume ratio of nanowires was observed after oxidation.

After the oxidation of 2min at $950^{\circ}C$, the cross-section view SEM image of $Si_{0.93}Ge_{0.07}$ and $Si_{0.89}Ge_{0.11}$ nanowires were shown in Figure 3-11 and 3-12. The area and surface-to-volume ratio were also summarized in the Table 3-3. After this oxidation process, the surface-to-volume ratio of nanowires also increased.

Due to the surface-to-volume ratio increase, the change of electric property will increase. This is a reason that enhancement of the sensitivity.

3.2 The sensitivity of SiGe nanowire sensor with various oxidation temperatures

In this section, we reported the electric property and the sensitivity of SiGe nanowire sensor with various oxidation temperatures. And, we discussed the result respectively.
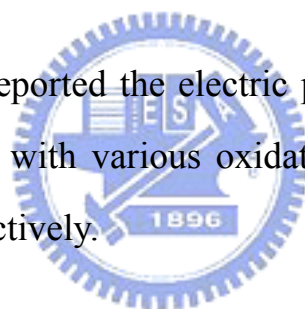
3.2.1 Mechanism of detecting IgG antibody

First, we used amino-propyl-trimethoxy-silane (APTMS) to modify the surface of native oxide layer around the SiGe nanowires. Due to hydroxyl molecules of the surface of native oxide layer were replaced by the methoxy side of the APTMS molecules, the surface potential of SiGe nanowire will increase. Therefore, the conductance of SiGe nanowires will increase. Next, we used bis-sulfo-succinimidyl suberate (BS3) as linker. When BS3 molecules bond to APTM molecules, the BS3 molecules was easier to release the sodium ion and break the single bond between the carbon atom and the oxygen atom. The reasons caused the

negative charge absorbing on the surface. Hence, the conductance of SiGe nanowires will decrease. Finally, the IgG antibody will bond to BS3 molecules. The conductance of SiGe nanowires will increase. The schema of mechanism was shown in Figure 3-13.

3.2.2 The sensitivity of SiGe nanowires without oxidation

In order to obtain the base data, we measured unoxidized-SiGe nanowires with different concentration. When different chemical molecules were dropped on the surface of SiGe nanowires, the I_D-V_D curve was recorded by *HP4156A*, as shown in Figures 3-14~3-17. In order to compare the sensitivity SiGe nanowire with/without oxidation, the value $\Delta S/S$ is considered. ΔS is the variation of conductance and S is the normal conductance of SiGe nanowire. The value shows the percentage change of conductance in the same change of surface potential after the APTMS and BS3 modified. We utilized equation 3.1 to obtain the average conductance of SiGe nanowires between V_D= 4V to V_D= 8V.

$$\text{Conductance} = \frac{\Delta I}{\Delta V} = \sigma \frac{W}{L} \qquad (3.1)$$

σ is the conductivity (S/m), W is the area of the nanowire, L is the length of the nanowire. We fixed the voltage ΔV at 0.2V to be constant. Figure 3-18 shows the result after APTMS, BS3 and IgG modified. The normal symbol is the conductance in the beginning and the APTMS symbol shows the conductance after APTMS modified. It is observed that higher conductance obtain after APTMS modified, the amounts of the APTMS molecules binding on the oxide surface performed like a constant voltage applied on the $Si_{0.93}Ge_{0.07}$ nanowire. The conductance of

BS3 became lower after BS3 linked. Finally, the antibody immunoglobulin IgG (protein) molecules were applied to link after the BS3 molecules, which also provided a positive gate voltage of the N-type $Si_{0.93}Ge_{0.07}$ nanowire. Figures 3-19~3-21 shows the conductance of the $Si_{0.89}Ge_{0.11}$, $Si_{0.8}Ge_{0.2}$, $Si_{0.7}Ge_{0.3}$ and $Si_{0.6}Ge_{0.4}$ respectively. The same phenomenon was also observed in other the SiGe nanowire with different Ge concentration. Finally, we utilized equation 3.2 to calculate change in conductivity after dropping different chemical molecules.

$$\text{Percentage of change of conductivity (\%)} = \frac{S_f - S_i}{S_i} \times 100\% \quad (3.2)$$

S_i is the conductance of SiGe nanowire before dipping chemical molecules, S_f is the conductance of SiGe nanowire after dipping chemical molecules. The value shows the percentage change of conductance in the same change of surface potential after the APTMS and BS3 modified. Figure 3-22 shows the percentage change of SiGe nanowire after APTMS modified. It is easily found that higher percentage change in conductance for the SiGe nanowire with higher Ge concentration. The higher variation appears in the same APTMS modified. The Ge enhances the sensitivity within the concentration from 7% to 30%. Figure 3-23 and 3-24 show the percentage change after BS3 and IgG modified. The same phenomenon that Ge enhances the sensitivity is also observed. The result is the same as our previous study for pH sensor.

3.2.3 The sensitivity of SiGe nanowires after the oxidation of 2 min at 900℃

To improve the sensitivity of SiGe nanowires with lower Ge

concentration, we utilized Ge condensation technology to enhance the Ge concentration in SiGe nanowire. The oxidation for the condition of 2 min. 900 ℃ was employed before the ion implantation, the I_D-V_D curve of SiGe nanowires were shown in figures 3-25~3-27 for the SiGe with different concentration. Similarly, we used formula 3.1 to calculate the average conductance of SiGe nanowires between V_D= 4V to V_D= 8V, as shown in Figures 3-28~3-30. Finally, we utilized formula 3.2 to calculate sensitivity of nanowires with different Ge concentration, as shown in Figures 3-31~3-32.

It is observed that the sensitivity of SiGe nanowires was enhanced by oxidation process. There are two reasons lead to the result. One is enhancement of surface-to-volume ratio after oxidation. The other one is Ge atom is rejected from the oxide and condensed in the remaining SiGe nanowire. In addition, $Si_{0.6}Ge_{0.4}$ nanowire was over oxidized because oxidation rate of SiGe layer increases with Ge concentration [48].

3.2.4 The sensitivity of SiGe nanowires after the oxidation of 2 min at 950℃

We expected the sensitivity of SiGe nanowires were further enhanced by oxidation. Therefore, we change temperature of oxidation process (T=950℃). Unfortunately, some of nanowires were failure ($Si_{0.8}Ge_{0.2}$, $Si_{0.7}Ge_{0.3}$ and $Si_{0.6}Ge_{0.4}$), the reason may be nanowires were over oxidized.

After the oxidation of 2min at 950℃, the I_D-V_D curve of SiGe nanowires were shown in Figures 3-33~3-34. The average conductance of

SiGe nanowires between V_D= 4V to V_D= 8V, was shown in Figure 3-35~3-36. Finally, the sensitivity of SiGe nanowires were shown in Figures 3-37~3-38.

We observed that the sensitivity of SiGe nanowire was enhanced by oxidation condition. After the oxidation of 2min at 950℃, the sensitivity of $Si_{0.93}Ge_{0.07}$ nanowire was enhancement as compared with the oxidation of 2min at 900℃. The result was shown in Figures 3-39~3-41. But, the sensitivity of $Si_{0.89}Ge_{0.11}$ nanowire was reduction as compared with the oxidation of 2min at 900℃. The result was shown in Figures 3-42~3-43. The reason may be higher defect was formed during this oxidation process [46]. In addition, we also oxidized SiGe nanowires by higher temperature (T=1000℃). But, oxidation rate was too fast so that nanowires were over oxidized.
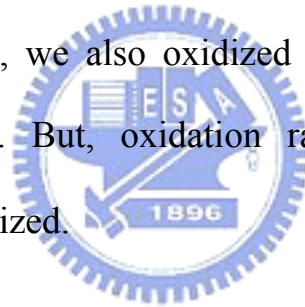
Chapter 4

Conclusions

We have successfully fabrication the SiGe nanowire with different Ge concentration respectively. In addition, we used the SiGe nanowires as bio-sensor. The 3-amino-propyl-trimethoxy-silane (APTMS) was used to modify the surface, which could connect the bio-linker. The conductance of SiGe nanowire increases owing to APTMS with positive charge. The bis (sulfosuccinimidyl) suberate sodium (BS3) as the bio-linker connected to APTMS and the conductance decreased because of negative charge. Finally, the protein immunoglobulin G (IgG) is linked to BS3, and the conductance reduces for negative charge. In order to compare the sensitivity with/without oxidation, the $\Delta S/S$ is considered. ΔS is the variation of conductance and S is the normal conductance of SiGe nanowire. We have demonstrated that the sensitivity was improved by using higher Ge concentration (7% ~ 30%) nanowire.

After the oxidation of 2 min at 900℃, the sensitivity of SiGe nanowires were enhanced. There are two reasons lead to the result. One is enhancement of surface-to-volume ratio after oxidation. The other one is Ge atom is rejected from the oxide and condensed in the remaining SiGe nanowire. In addition, we observed that oxidation rate of SiGe nanowire increase with Ge concentration. Therefore, $Si_{0.6}Ge_{0.4}$ nanowire was oxidized over.

After the oxidation of 2 min at 950℃, the sensitivity of $Si_{0.93}Ge_{0.07}$ nanowires were enhanced. The percentage change of the conductance is

9.6% for the normal state, 13.9% for the 900 ℃ oxidation and 34.76% for 950 ℃ oxidation after APTMS modified. It is clearly observed that the sensitivity is improved by oxidation. After the oxidation of 2min at 950℃, the sensitivity (22.27%) of $Si_{0.89}Ge_{0.11}$ nanowire was reduction as compared with the oxidation (36.36%) of 2min at 900℃. The reason may be that higher defect was formed during this oxidation process. In addition, we also oxidized SiGe nanowires by higher temperature (T=1000℃). But, oxidation rate was too fast so that nanowires were over oxidized.

Chapter 5

Future Work

Due to oxygen concentration will affect whether GeO_2 formed during oxidation process. We will change nitrogen/oxygen ratio to avoid GeO_2 formed. In addition, we can change time of oxidation to control Ge concentration in SiGe nanowires. By changing nitrogen/oxygen ratio and time of oxidation, we will obtain optimum condition of oxidation.

Material of nanowire sensor	Application
Silicon	pH sensor,bio-sensor,DNA sensor and virus sensor
Metal oxide	gas sensor
Polymer	gas sensor
Metal	gas sensor

Table 1-1
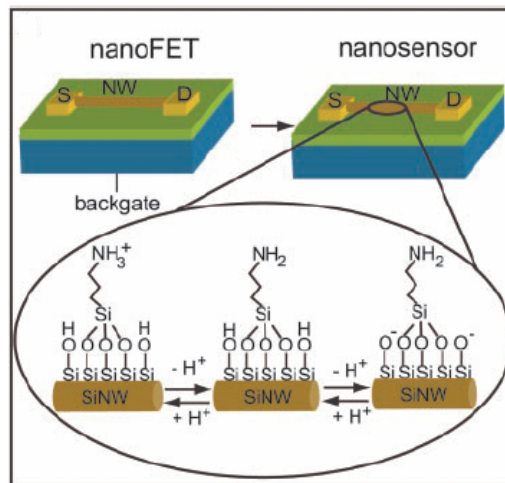
Figure 1-1. Conversion of a NW FET into NW nanosensor for pH sensing [1].
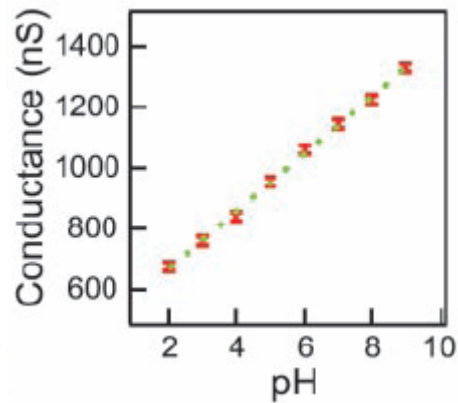
Figure 1-2. Plot of the conductance Versus pH [1].
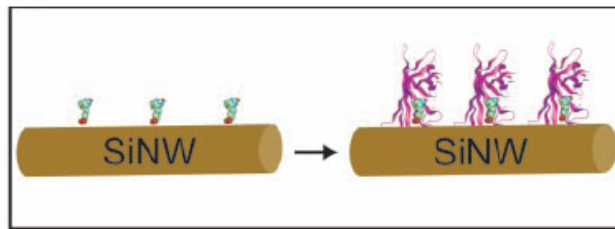
Figure 1-3. A biotion-modified SiNW and subsequent binding of streptavidin to the SiNW surface [1].
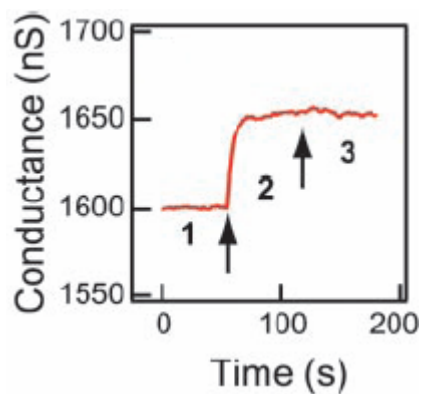
Figure 1-4. Plot of conductance versus time for a biotin-modified SiNW,where region 1 correspond to buffer solution,region 2 corresponds to the addition of 250nM streptavidin [1].
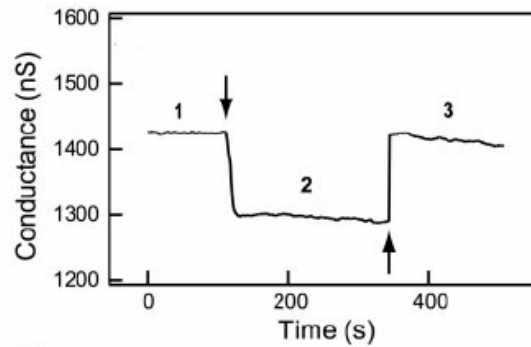
Figure 1-5. Conductance versus time for a biotin-modified SiNW,where region 1 corresponds to buffer solution, region 2 corresponds to the addition of ~3 μ M m-antibiotin,and region 3 corresponds to pure buffer solution [1].
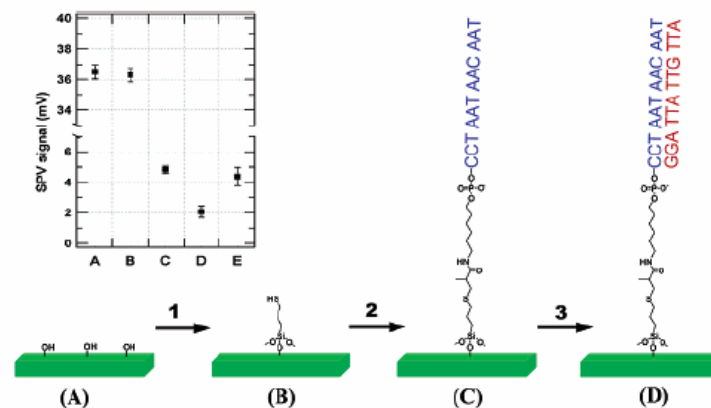
Figure 1-6. Modification scheme of the SiNW surface for the DNA detector: (1) self-assembly of 3-mercaptopropyltrimethoxysilane (MPTMS) by gas-phase reaction in Ar for 4 h; (2) covalent immobilization of DNA probes by exposing the previous surface to 5 iM solution of oligonucleotide CCT AAT AAC AAT modified with acrylic phosphoramidite at the 5¢-end for 12 h; (3) DNA detection based on hybridization between label-free complementary DNA target GGA TTA TTG TTA and the immobilized DNA probes on the SiNW surfaces. The inset is the SPV signal on a p-type Si surface at different stages of the modification; A, B, and C correspond to the schematic diagrams, D is with 25 pM solution of complementary DNA target exposed to the surface C, and E is with 25 pM solution of noncomplementary DNA (GGA TCA TTG TTA) exposed to the surface C [10].
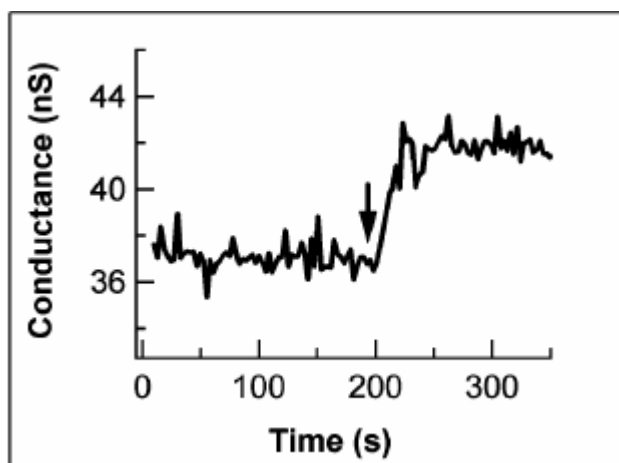
Figure 1-7. Conductance of the same p-type SiNW, where the arrow indicates the addition of 25 pM complementary DNA (GGA TTA TTG TTA) solution [10].
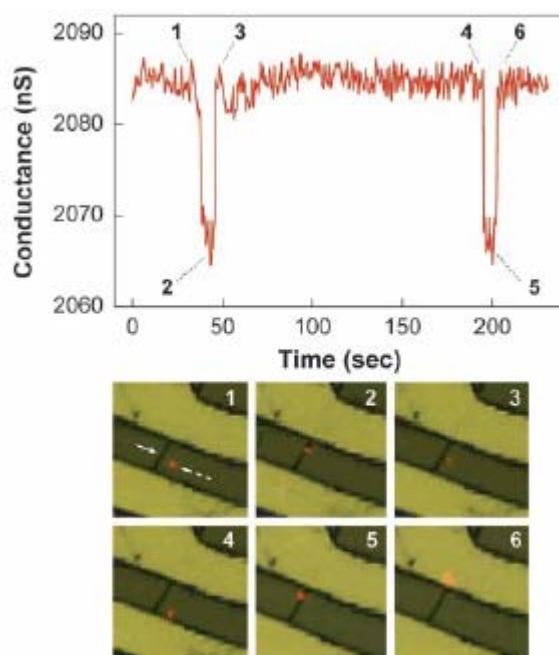
Figure 1-8. Conductance (Upper) and optical (Lower) data recorded simultaneously vs. time for a single silicon nanowire device after introduction of influenza A solution. Combined bright-field and fluorescence images correspond to time points 1–6 indicated in the conductance data; virus appears as a red dot in the images [11].
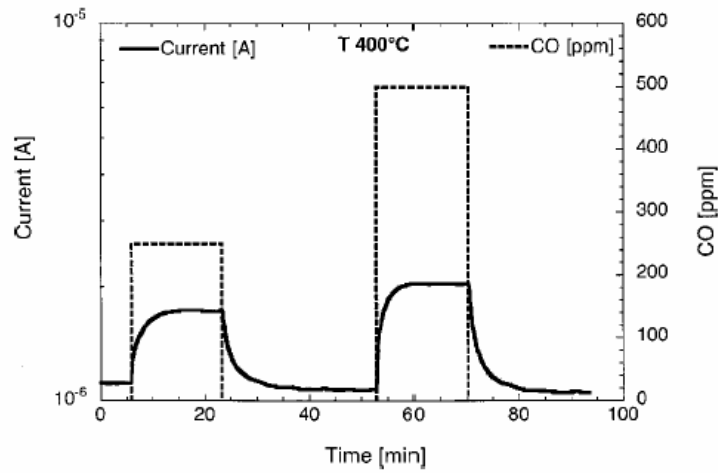
Figure 1-9. Response of the SnO2 nanobelts to CO at a working temperature of 400 °C and 30% RH [13].
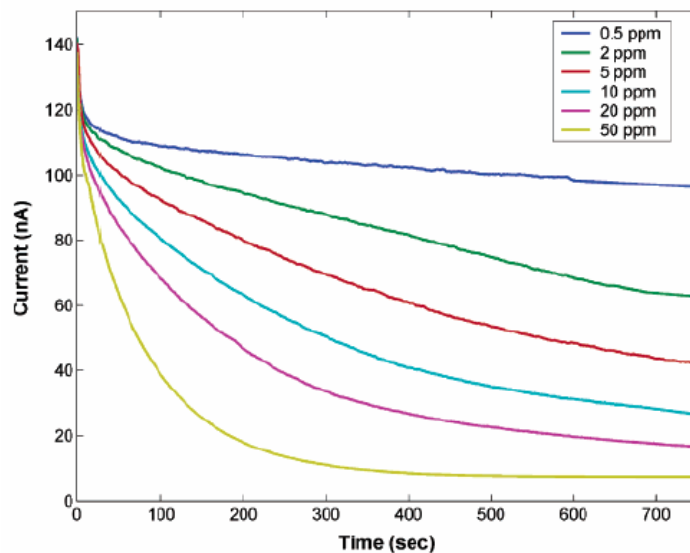
Figure 1-10. Measured time-dependent current through an individual CPNW sensor upon exposure to NH3 gas. The nanowire device being tested was about 335 nm in diameter [16].
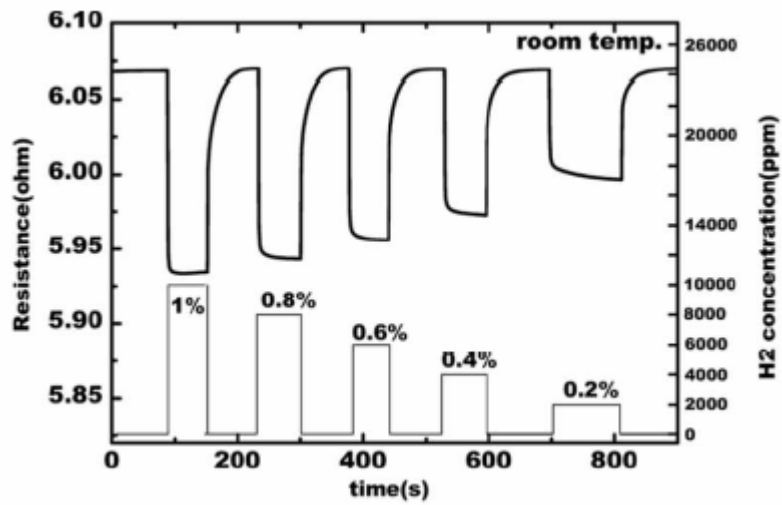
Figure 1-11. Sensor resistance responses for hydrogen concentration varied in a range from 0.2 to 1% by pulses [18].
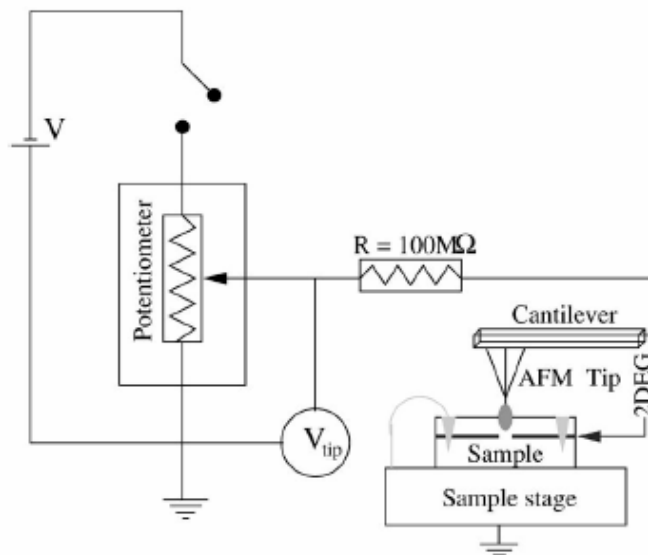
Figure 1-12. Schema of Scanning Probe Lithography (SPL).
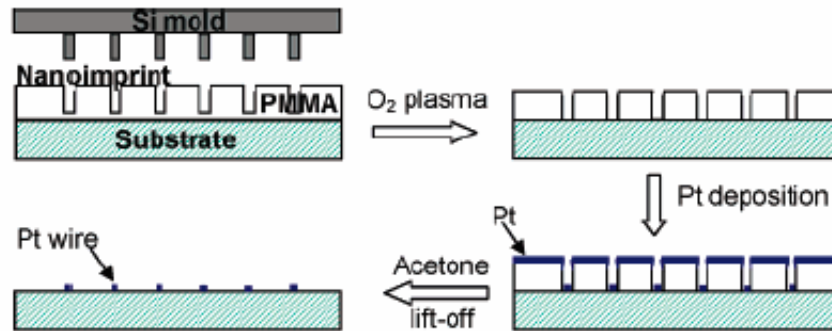
Figure 1-13. Schema of imprint process [28].
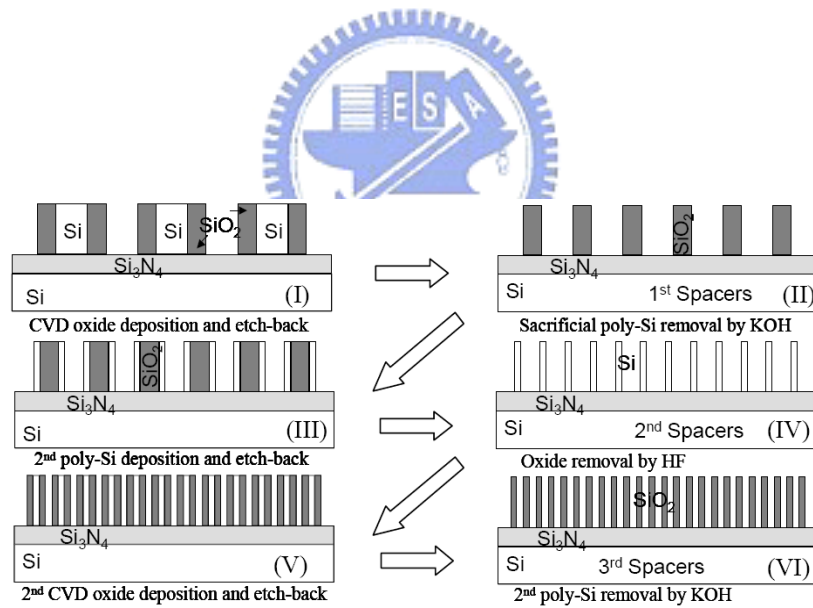
Figure 1-14. Schematic view of iterative spacer lithography (ISL) [29].
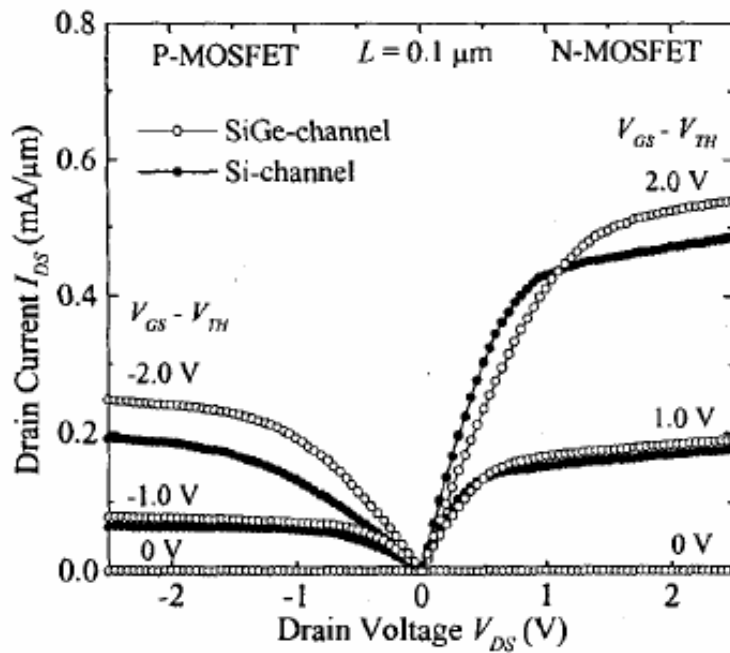
Figure 1-15. Drain current of N- and P-MOSFETs are improved with the use of SiGe-channel [33].
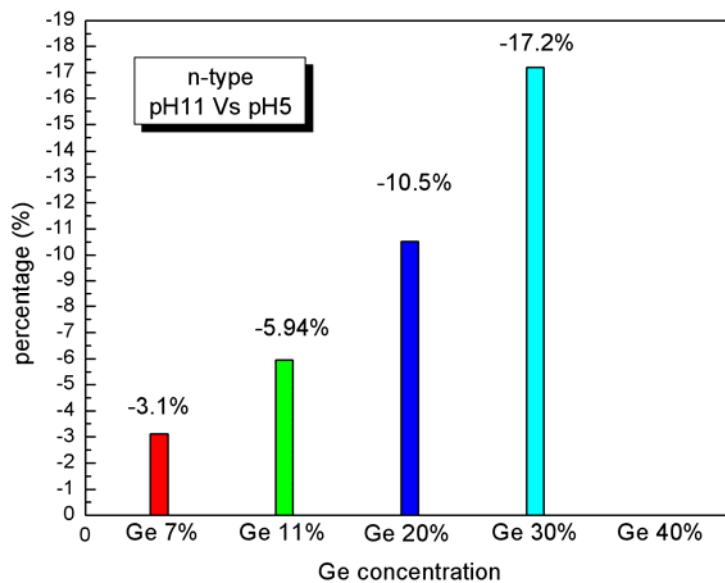
Figure 1-16. The N-type sensitivity is improved with the increase concentration of Ge. [percentage % = (pH11-pH5)/pH5]
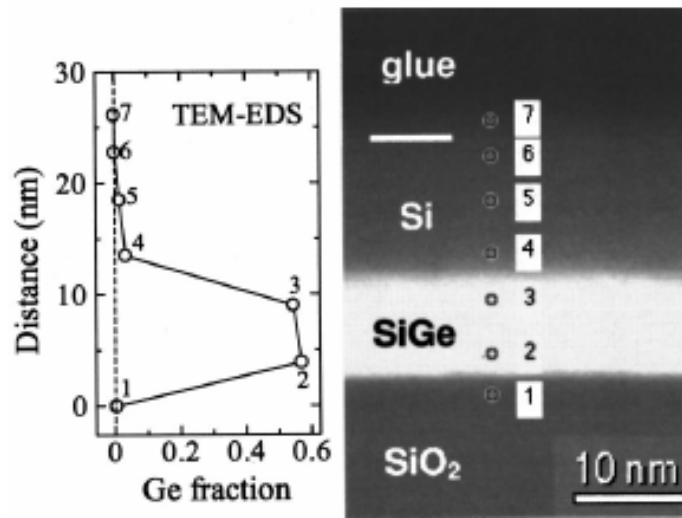
Figure 1-17. Scanning TEM image and Ge profile across the layers obtained by EDS measurement [41].
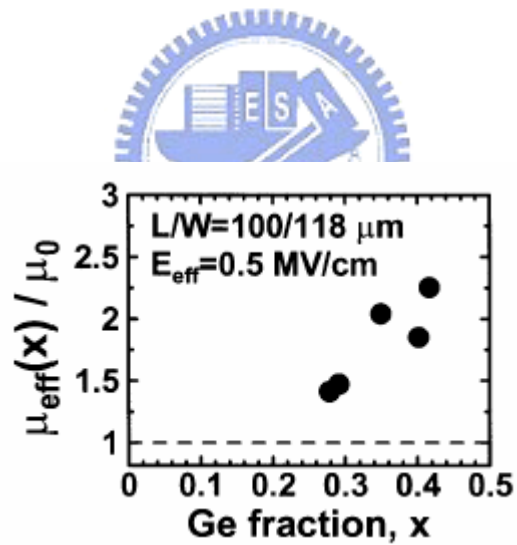
Figure 1-18. Mobility enhancement factor for the SGOI-MOSFETs as a function of the Ge fraction [47].
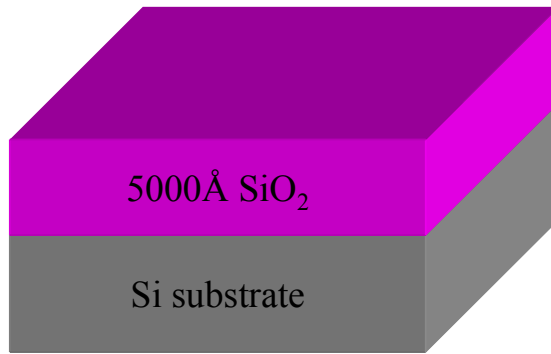
Figure 2-1. SiO$_2$ layer is grown on Si substrate. The thickness of SiO$_2$ layer is 5000Å.
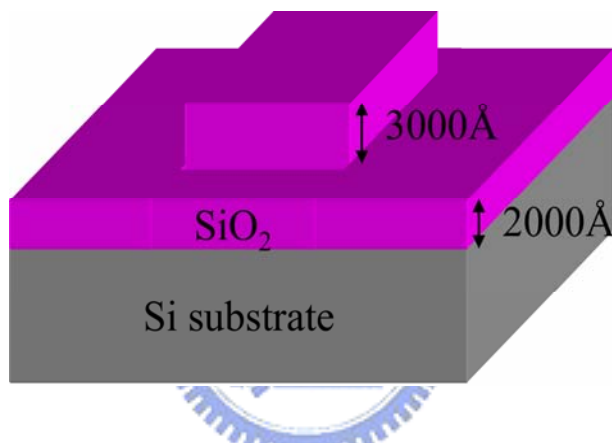
Figure 2-2. Defined active area. The height of oxide step is 3000Å.
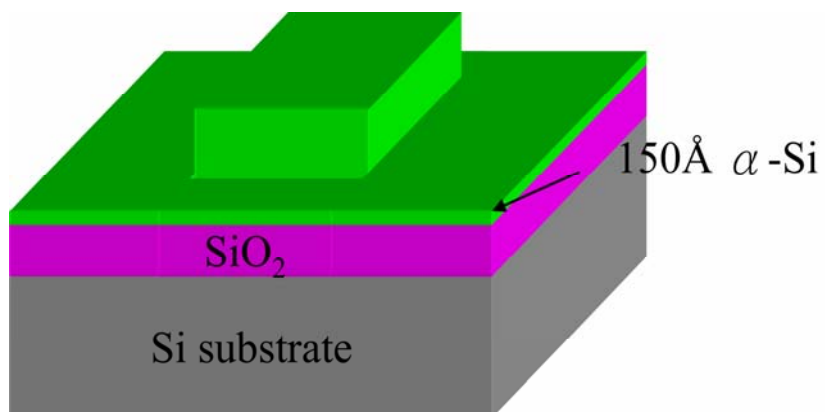
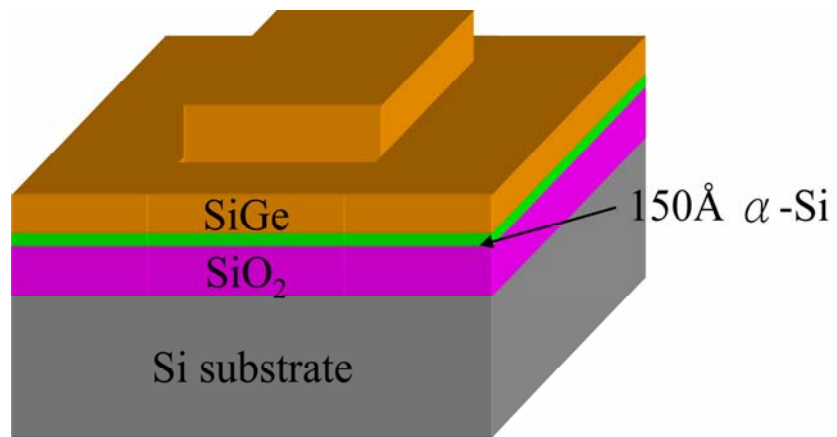Figure 2-3. Amorphous Si layer is deposited on SiO$_2$ layer. The thickness ofα-Si layer is 150Å.
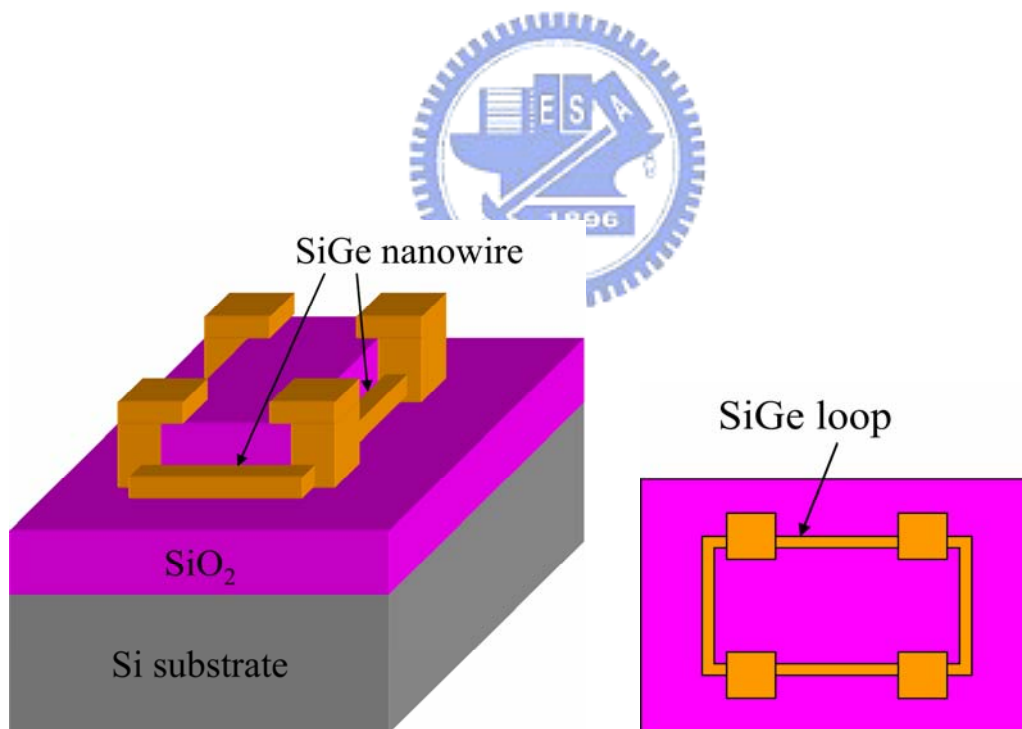
Figure 2-4. SiGe layer is deposited on α-Si layer.

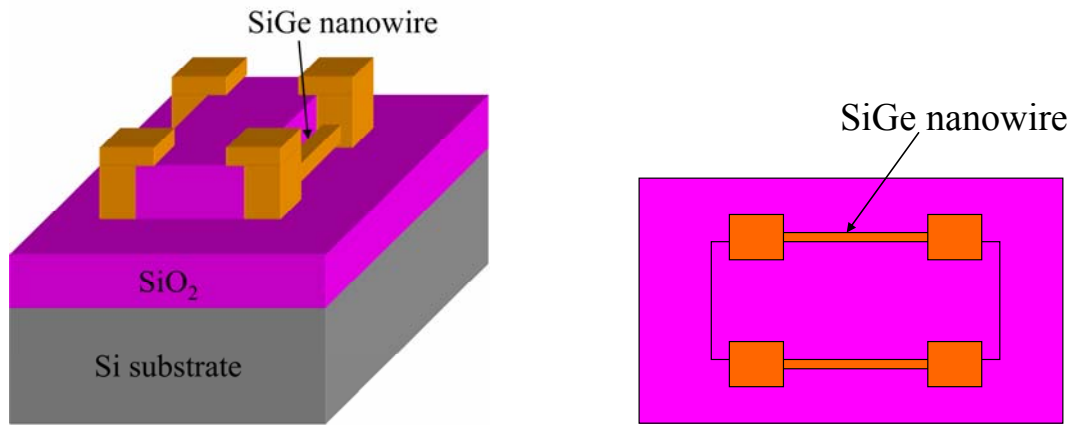Figure 2-5. Defined S/D region and nanowire.

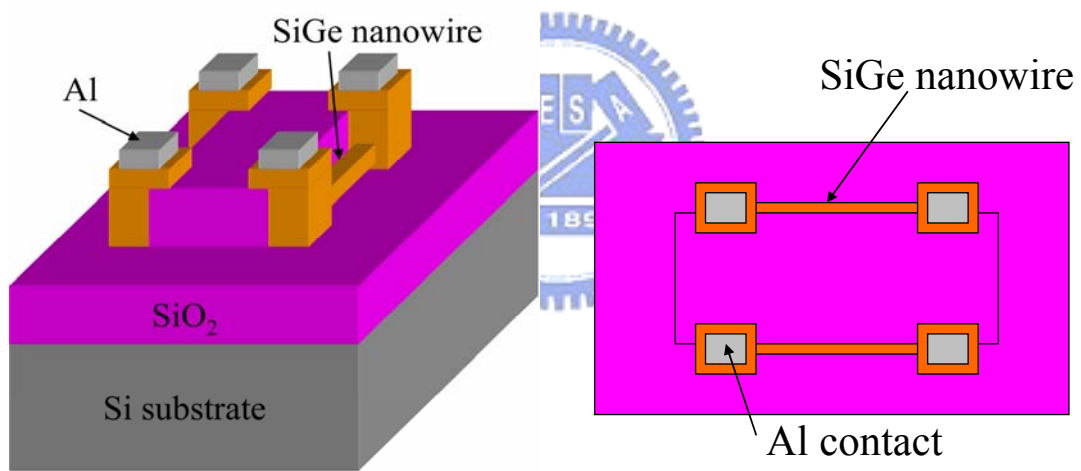Figure 2-6. Remove one side of the parallel SiGe spacer.
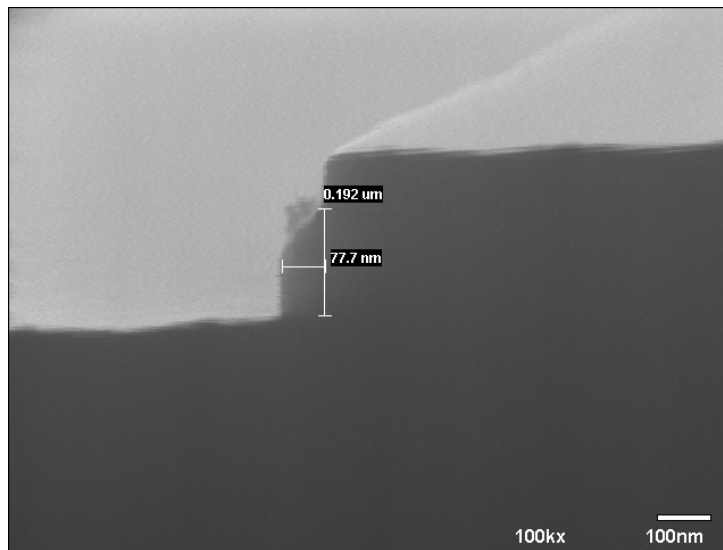

Figure 2-7. Defined Al contact pad.

Figure 3-1. The Cross-Section view of the SEM of $Si_{0.93}Ge_{0.07}$ nanowire. The height and width of $Si_{0.93}Ge_{0.07}$ nanowire are 192nm and 77nm respectively.
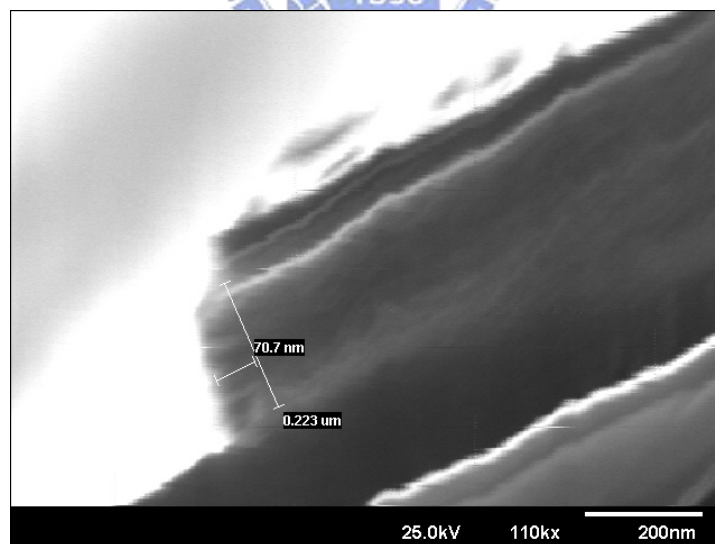

Figure 3-2. The Cross-Section view of the SEM of $Si_{0.89}Ge_{0.11}$ nanowire. The height and width of $Si_{0.89}Ge_{0.11}$ nanowire are 184nm and 45.5nm respectively.
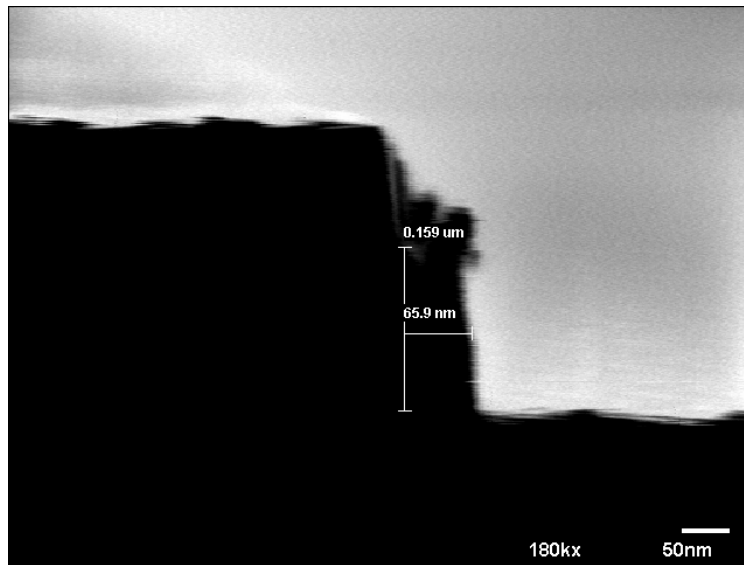
Figure 3-3. The Cross-Section view of the SEM of $Si_{0.8}Ge_{0.2}$ nanowire. The height and width of $Si_{0.8}Ge_{0.2}$ nanowire are 159nm and 65.9nm respectively.
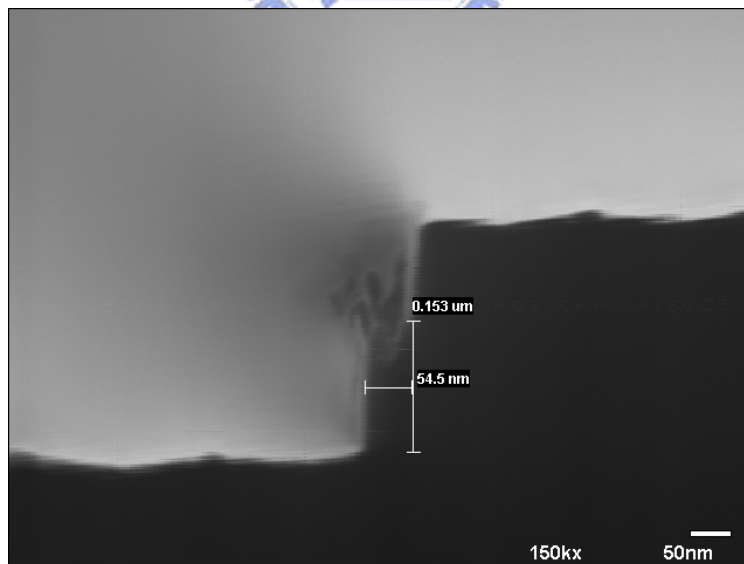

Figure 3-4. The Cross-Section view of the SEM of $Si_{0.7}Ge_{0.3}$ nanowire. The height and width of $Si_{0.7}Ge_{0.3}$ nanowire are 153nm and 54.5nm respectively.
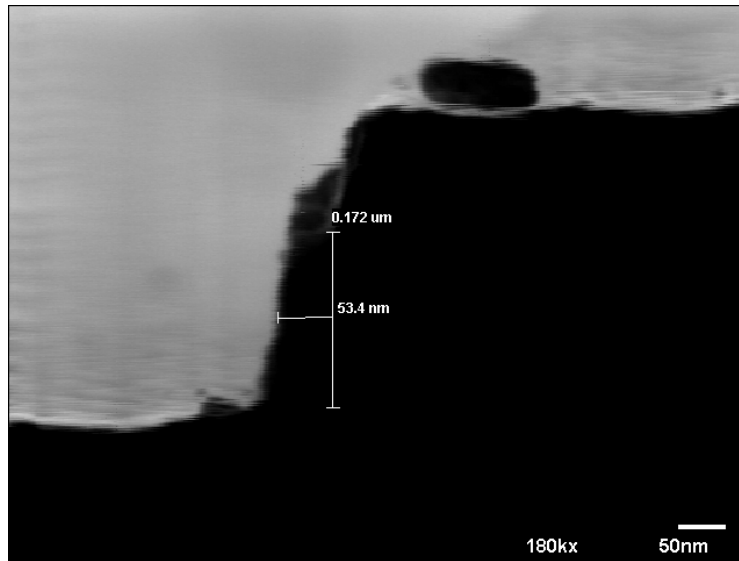
Figure 3-5. The Cross-Section view of the SEM of $Si_{0.6}Ge_{0.4}$ nanowire. The height and width of $Si_{0.6}Ge_{0.4}$ nanowire are 153nm and 54.5nm respectively.
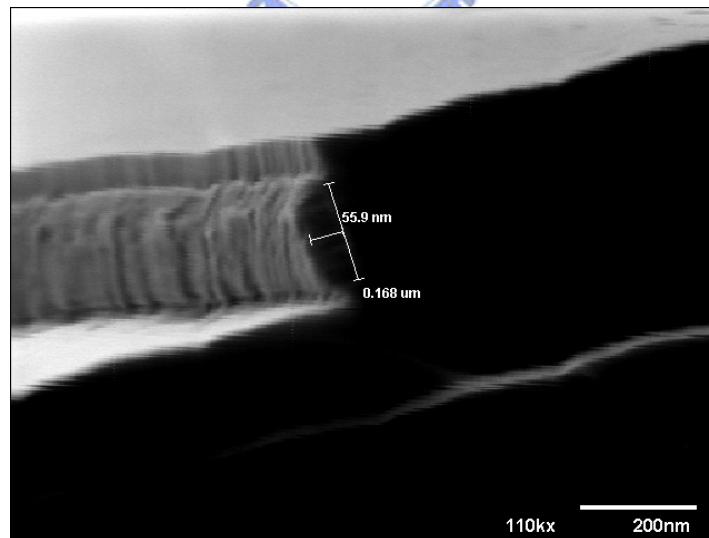

Figure 3-6. The Cross-Section view of the SEM of $Si_{0.93}Ge_{0.07}$ nanowire after the oxidation of 2 min at 900℃. The height and width of nanowire are 168nm and 55.9nm respectively.
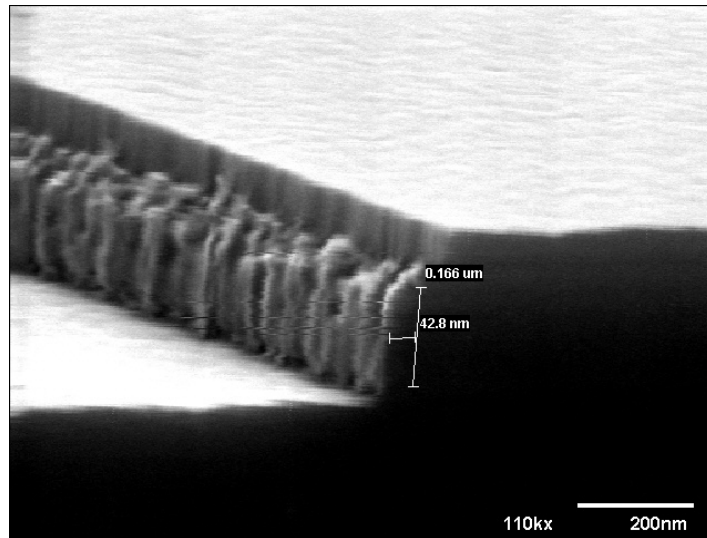
Figure 3-7. The Cross-Section view of the SEM of $Si_{0.89}Ge_{0.11}$ nanowire after the oxidation of 2 min at 900℃. The height and width of nanowire are 166nm and 42.8nm respectively.
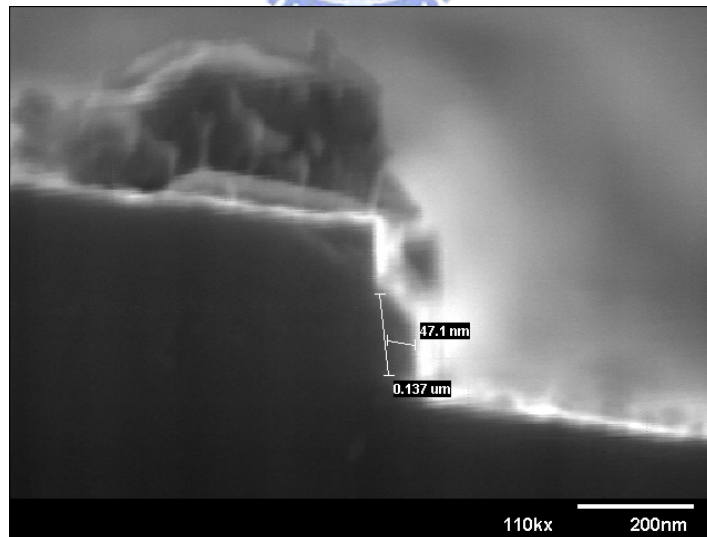

Figure 3-8. The Cross-Section view of the SEM of $Si_{0.8}Ge_{0.2}$ nanowire after the oxidation of 2 min at 900℃. The height and width of nanowire are 137nm and 47.1nm respectively.
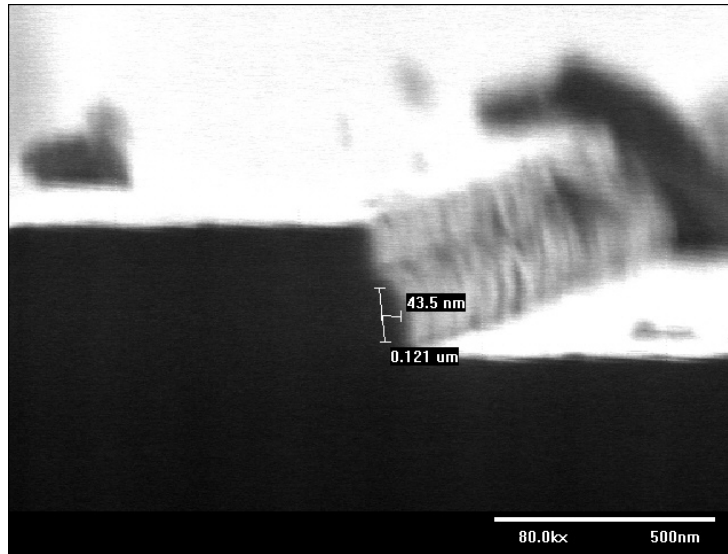
Figure 3-9. The Cross-Section view of the SEM of $Si_{0.7}Ge_{0.3}$ nanowire after the oxidation of 2 min at $900^{\circ}C$. The height and width of nanowire are 121nm and 43.5nm respectively.

Figure 3-10. The Cross-Section view of the SEM of $Si_{0.6}Ge_{0.4}$ nanowire after the oxidation of 2 min at $900^{\circ}C$. The nanowire was oxidized over.

Figure 3-11. The Cross-Section view of the SEM of $Si_{0.93}Ge_{0.07}$ nanowire after the oxidation of 2 min at 950℃. The height and width of nanowire are 155nm and 42.9nm respectively.

Figure 3-12. The Cross-Section view of the SEM of $Si_{0.89}Ge_{0.11}$ nanowire after the oxidation of 2 min at 950℃. The height and width of nanowire are 118nm and 38nm respectively.
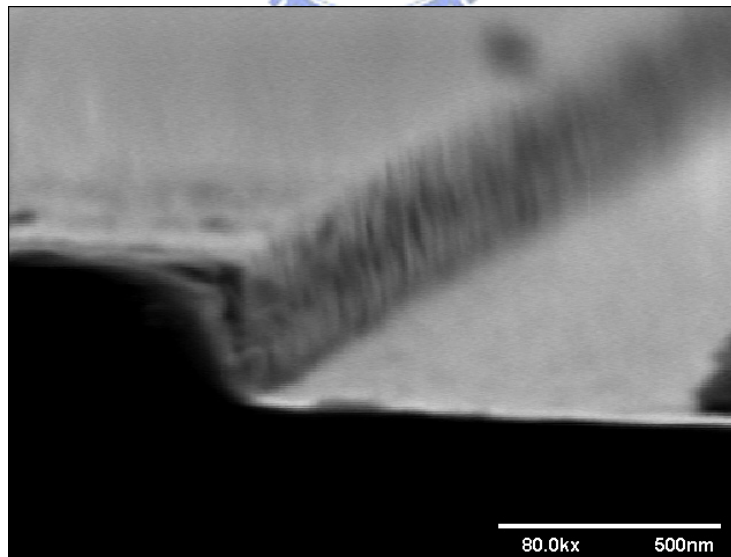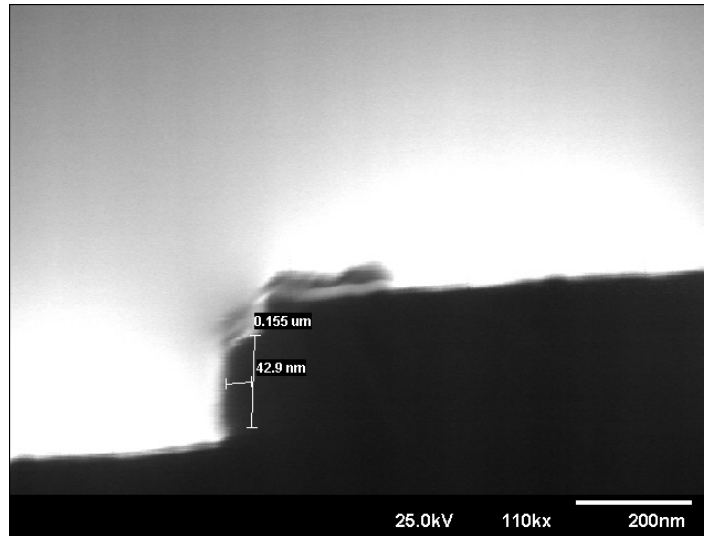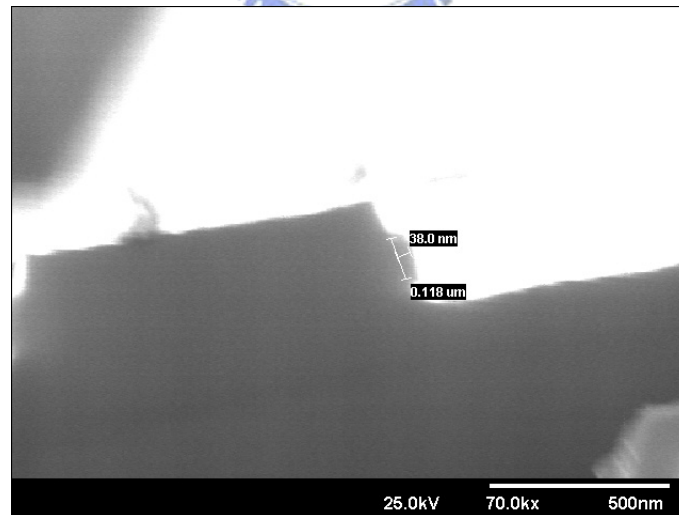
Unoxidation				
$Si_{1-x}Ge_x$	height	width	area	surface/volume
$Si_{0.93}Ge_{0.07}$	1.92E-07	7.77E-08	1.49E-14	1.81E+07
$Si_{0.89}Ge_{0.11}$	2.23E-07	7.07E-08	1.58E-14	1.86E+07
$Si_{0.8}Ge_{0.2}$	1.59E-07	6.59E-08	1.05E-14	2.14E+07
$Si_{0.7}Ge_{0.3}$	1.53E-07	5.45E-08	8.34E-15	2.49E+07
$Si_{0.6}Ge_{0.4}$	1.72E-07	5.34E-08	9.18E-15	2.46E+07

Table 3-1

Dry Oxidation of 2min at 900℃				
	height	width	area	surface/volume
$Si_{0.93}Ge_{0.07}$	1.68E-07	5.59E-08	9.39E-15	2.38E+07
$Si_{0.89}Ge_{0.11}$	1.66E-07	4.28E-08	7.10E-15	2.94E+07
$Si_{0.8}Ge_{0.2}$	1.37E-07	4.71E-08	6.45E-15	2.85E+07
$Si_{0.7}Ge_{0.3}$	1.21E-07	4.35E-08	5.26E-15	3.13E+07
$Si_{0.6}Ge_{0.4}$	-	-	-	-

Table 3-2

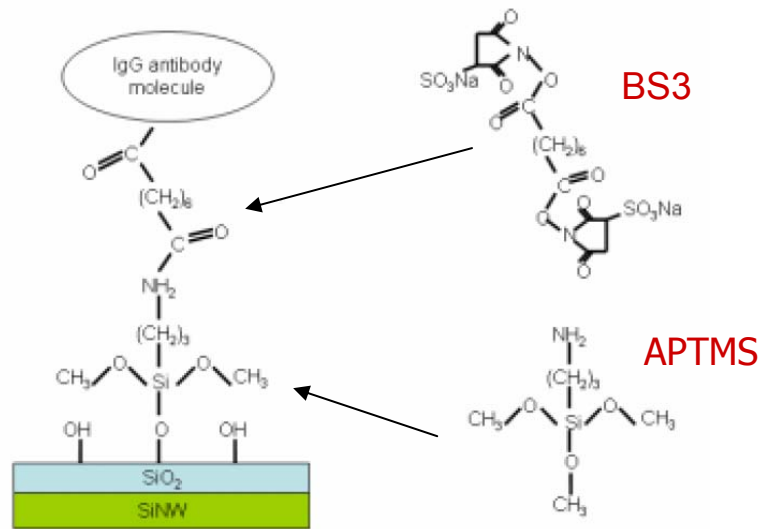| Dry Oxidation of 2min at 950℃				
	height	width	area	surface/volume
$Si_{0.93}Ge_{0.07}$	1.55E-07	4.29E-08	6.65E-15	2.98E+07
$Si_{0.89}Ge_{0.11}$	1.18E-07	3.80E-08	4.48E-15	3.48E+07
$Si_{0.8}Ge_{0.2}$	-	-	-	-
$Si_{0.7}Ge_{0.3}$	-	-	-	-
$Si_{0.6}Ge_{0.4}$	-	-	-	-

Table 3-3

Figure 3-13. Schema of mechanism of detecting IgG antibody.
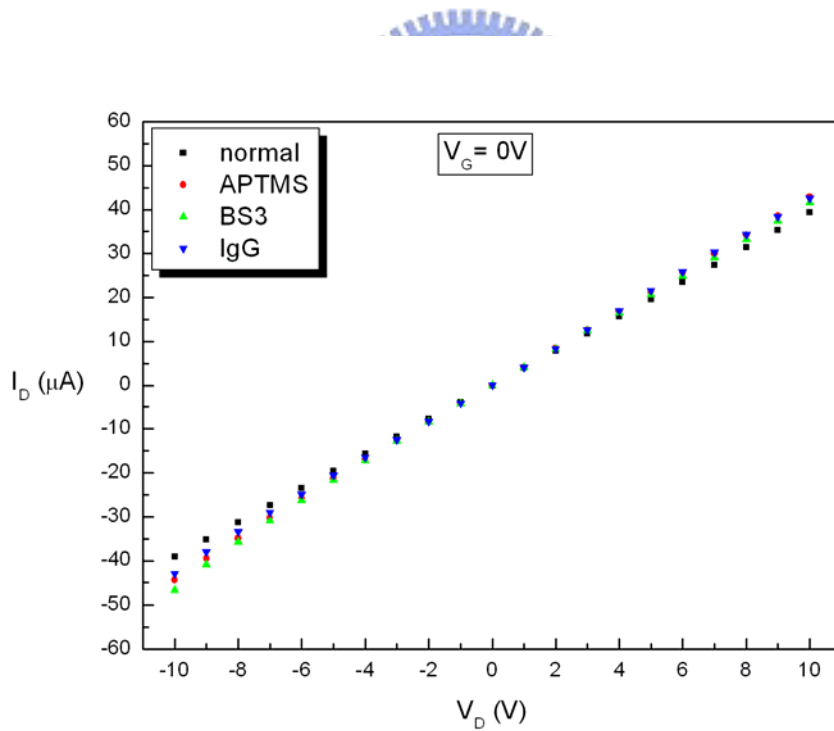

Figure 3-14. The I_D-V_D curve of N-type $Si_{0.93}Ge_{0.07}$ nanowire. The length of nanowire is 30 μ m.
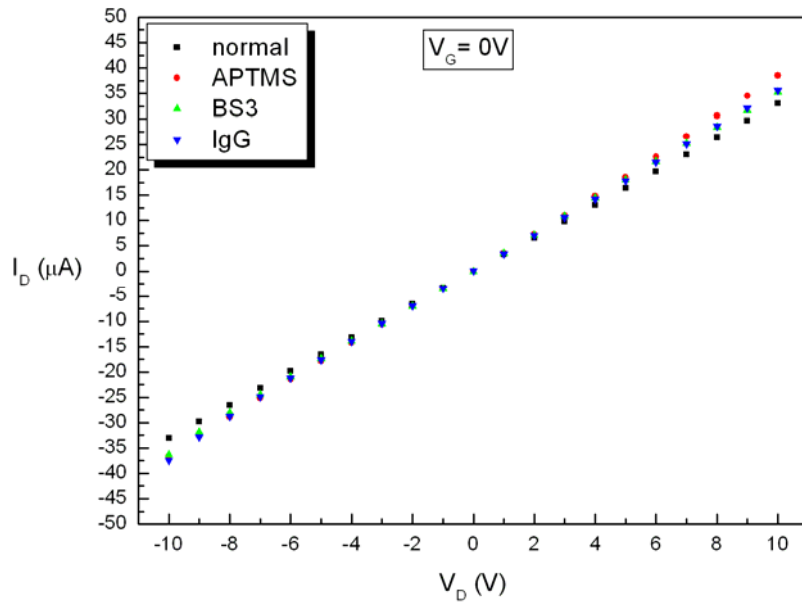
Figure 3-15. The I_D-V_D curve of N-type $Si_{0.89}Ge_{0.11}$ nanowire. The length of nanowire is 17μm.

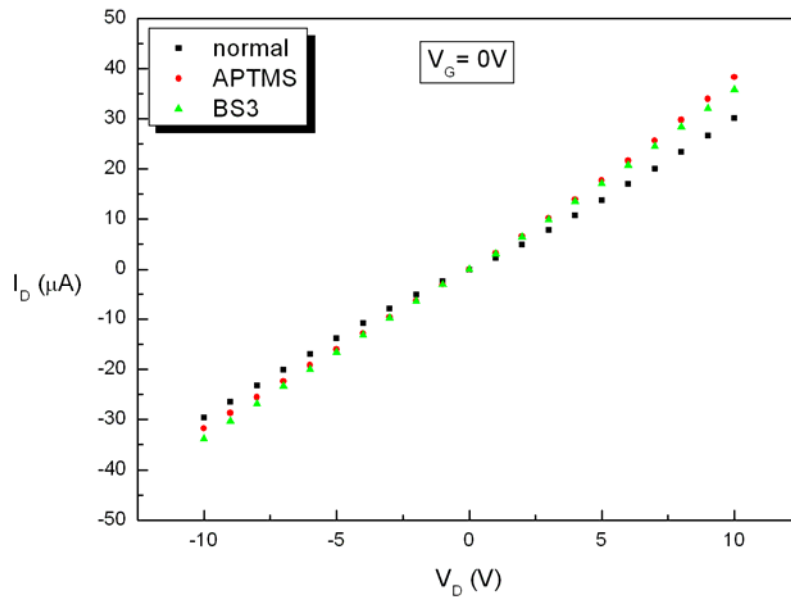Figure 3-16. The I_D-V_D curve of N-type $Si_{0.8}Ge_{0.2}$ nanowire. The length of nanowire is 13μm.
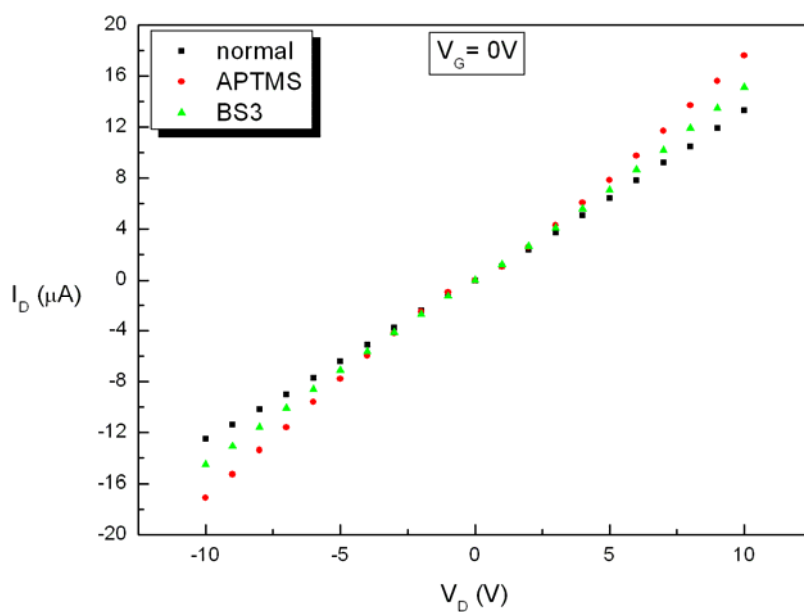
Figure 3-17. The I_D-V_D curve of N-type $Si_{0.7}Ge_{0.3}$ nanowire. The length of nanowire is 19 μ m.

Figure 3-18. The conductance of N-type $Si_{0.93}Ge_{0.07}$ nanowire changes with different chemical molecules. The length of nanowire is 30 μ m.

Figure 3-19. The conductance of N-type $Si_{0.89}Ge_{0.11}$ nanowire changes with different chemical molecules. The length of nanowire is 17 μ m.

Figure 3-20. The conductance of N-type $Si_{0.8}Ge_{0.2}$ nanowire changes with different chemical molecules. The length of nanowire is 13 μ m.

Figure 3-21. The conductance of N-type $Si_{0.7}Ge_{0.3}$ nanowire changes with different chemical molecules. The length of nanowire is 19 μ m.
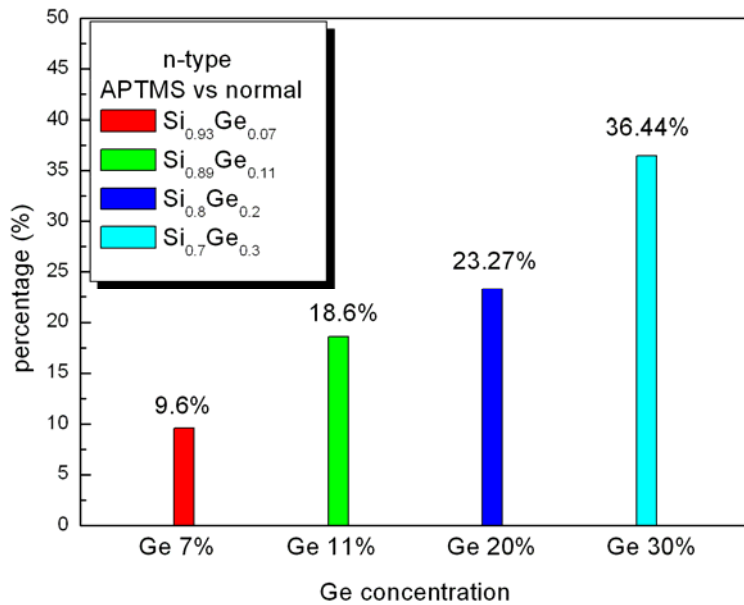
Figure 3-22. The sensitivity improves with the increment of Ge concentration.
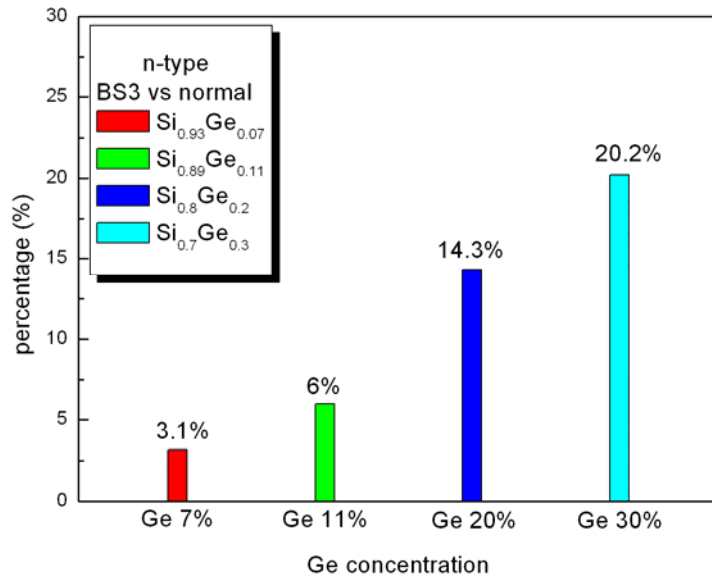
Figure 3-23. The sensitivity improves with the increment of Ge concentration.
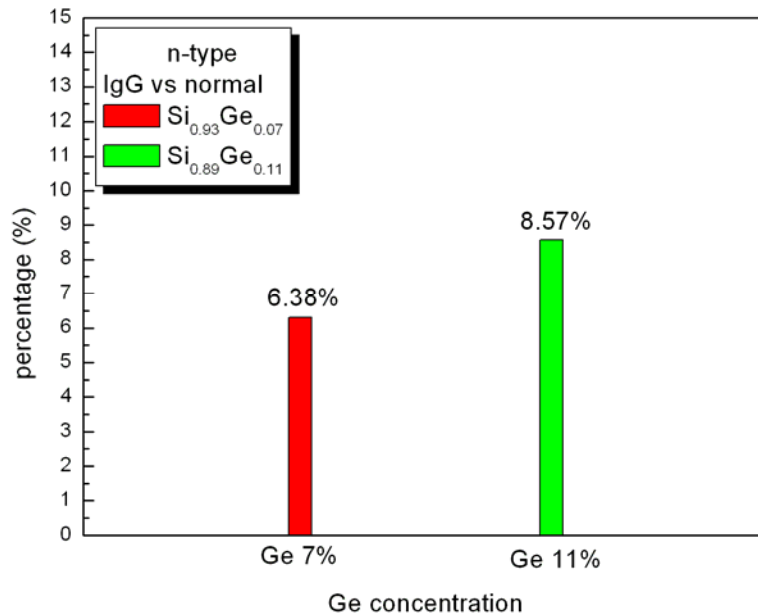
Figure 3-24. The sensitivity improves with the increment of Ge concentration.

Figure 3-25. After the oxidation of 2min at 900℃, I_D-V_D curve of N-type

$Si_{0.93}Ge_{0.07}$ nanowire. The length of nanowire is 50 μ m.

Figure 3-26. After the oxidation of 2min at 900℃, I_D-V_D curve of N-type

$Si_{0.89}Ge_{0.11}$ nanowire. The length of nanowire is 9 μ m.
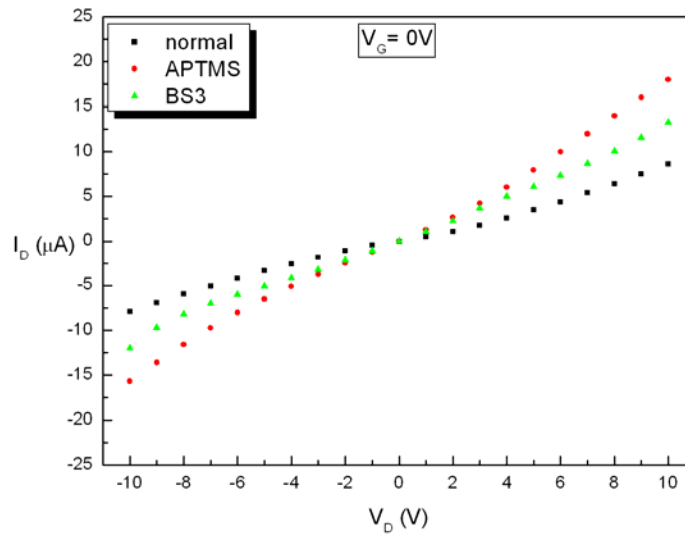
Figure 3-27. After the oxidation of 2min at 900℃, I_D-V_D curve of N-type

$Si_{0.8}Ge_{0.2}$ nanowire. The length of nanowire is 15 μ m.
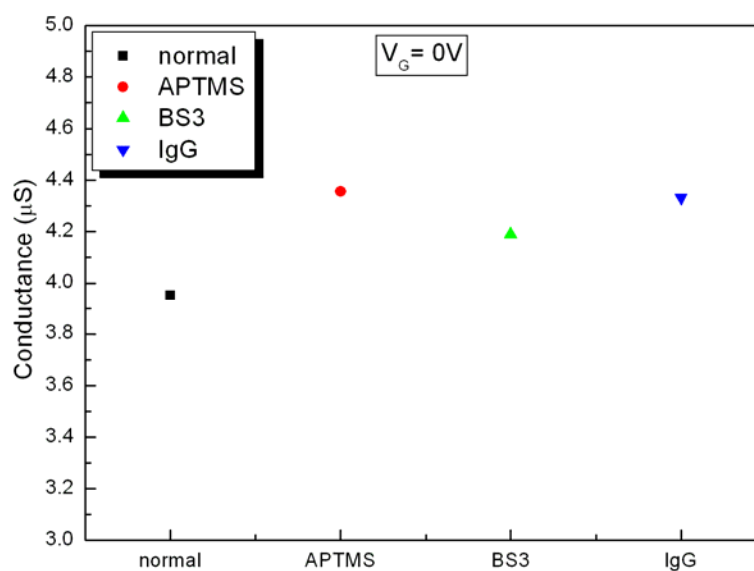

Figure 3-28. After the oxidation of 2min at 900℃, the conductance of

N-type $Si_{0.93}Ge_{0.07}$ nanowire changes with different chemical molecules.

The length of nanowire is 50 μ m.
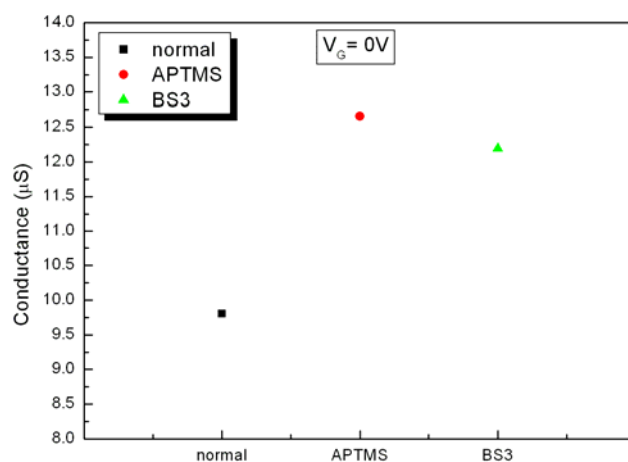
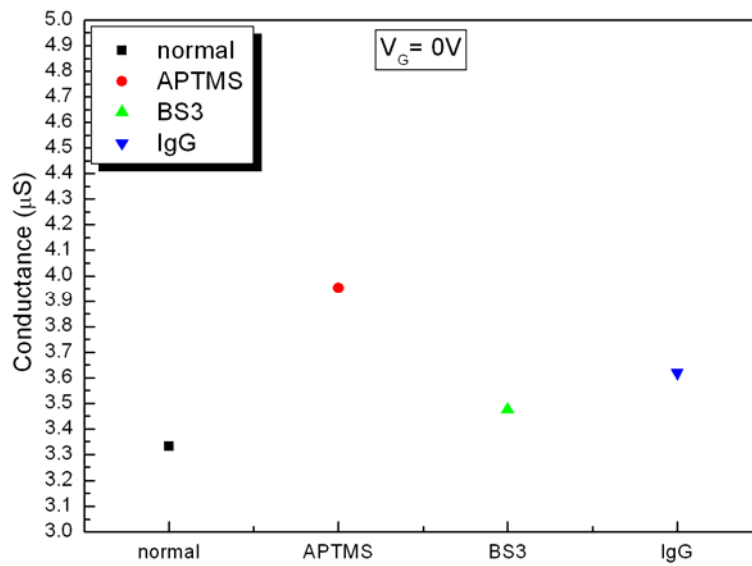Figure 3-29. After the oxidation of 2min at 900℃, the conductance of

N-type $Si_{0.89}Ge_{0.11}$ nanowire changes with different chemical molecules.
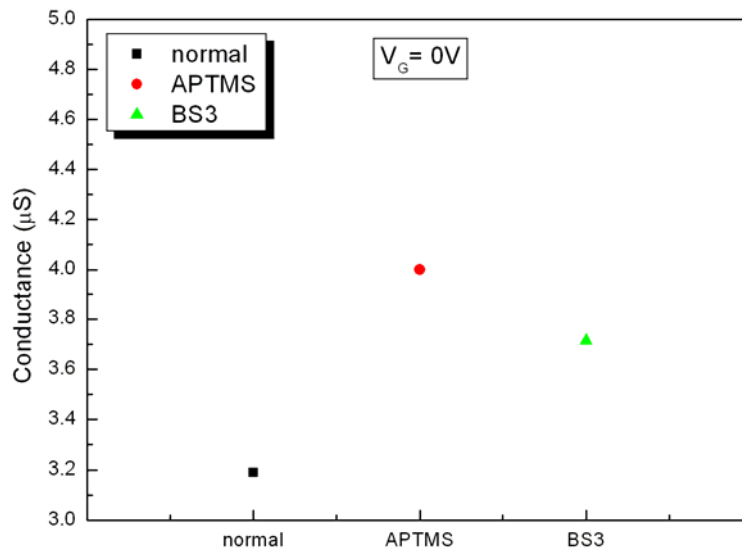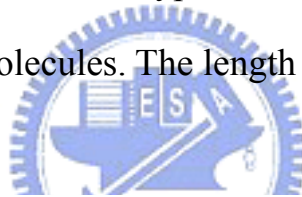
The length of nanowire is 7 μ m.
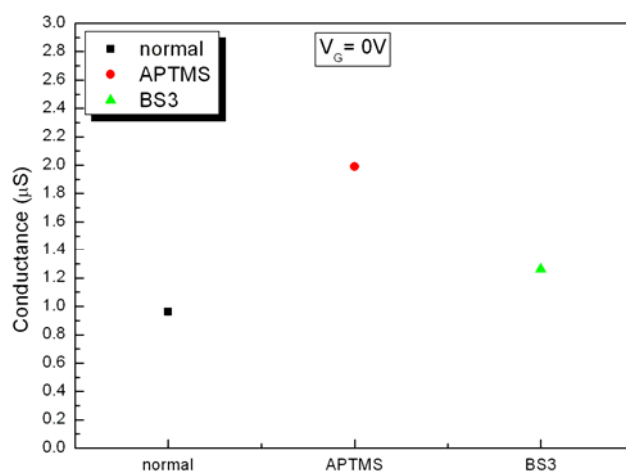
Figure 3-30. After the oxidation of 2min at 900℃, the conductance of

N-type $Si_{0.8}Ge_{0.2}$ nanowire changes with different chemical molecules.
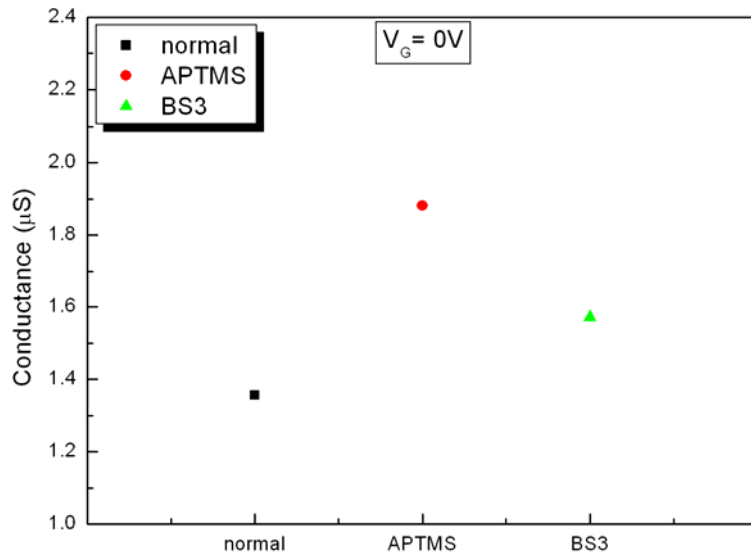
The length of nanowire is 15 μ m.
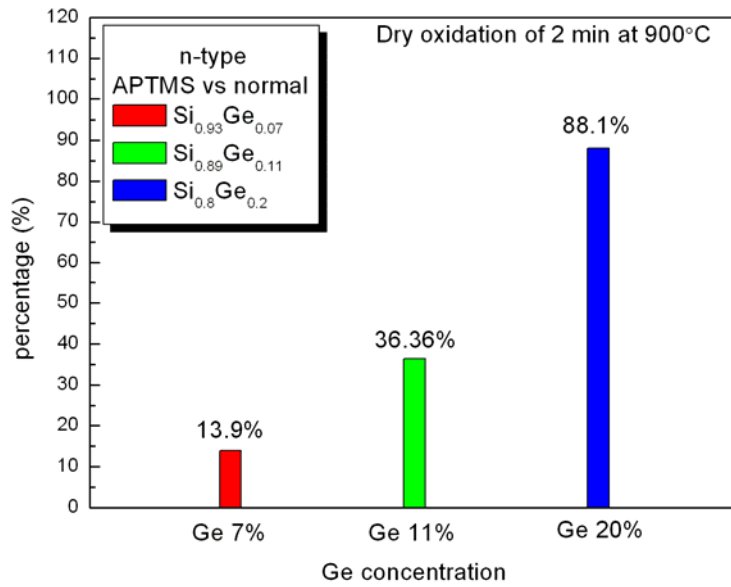
Figure 3-31. After the oxidation of 2min at 900℃, the sensitivity of SiGe

nanowires were enhanced.
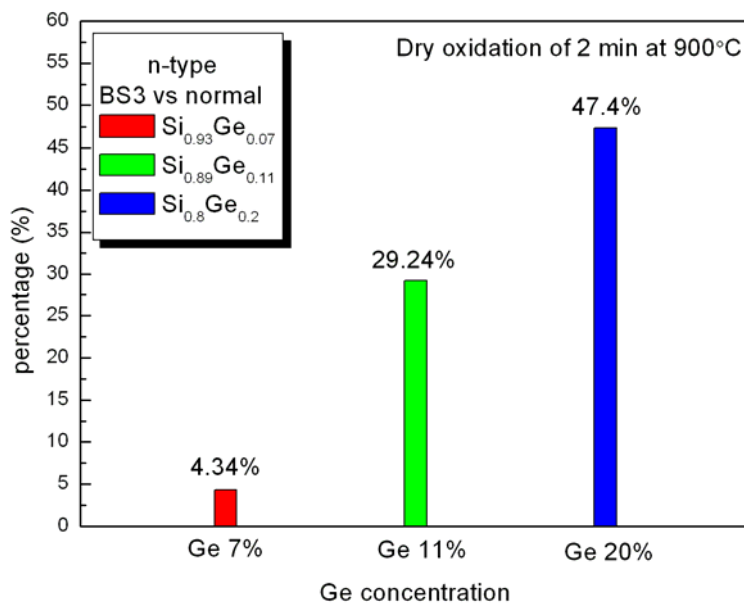
Figure 3-32. After the oxidation of 2min at 900℃, the sensitivity of SiGe

nanowires were enhanced.
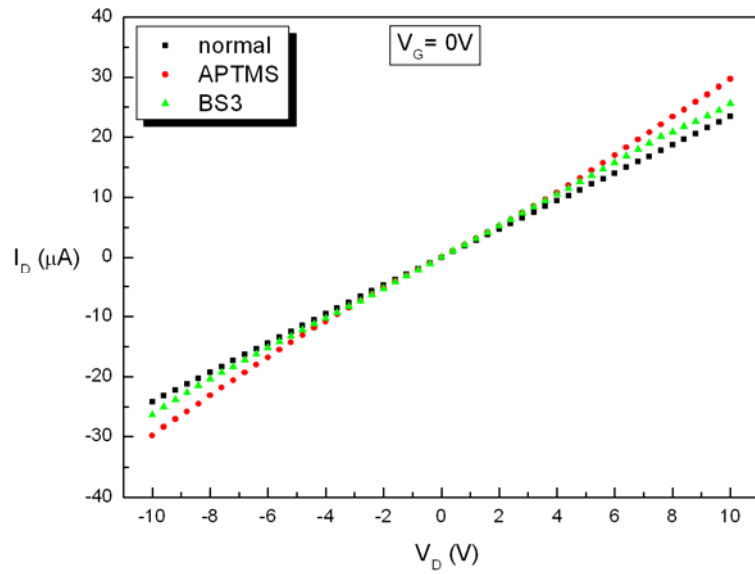
Figure 3-33. After the oxidation of 2min at 950℃, I_D-V_D curve of N-type

$Si_{0.93}Ge_{0.07}$ nanowire. The length of nanowire is 20 μ m.
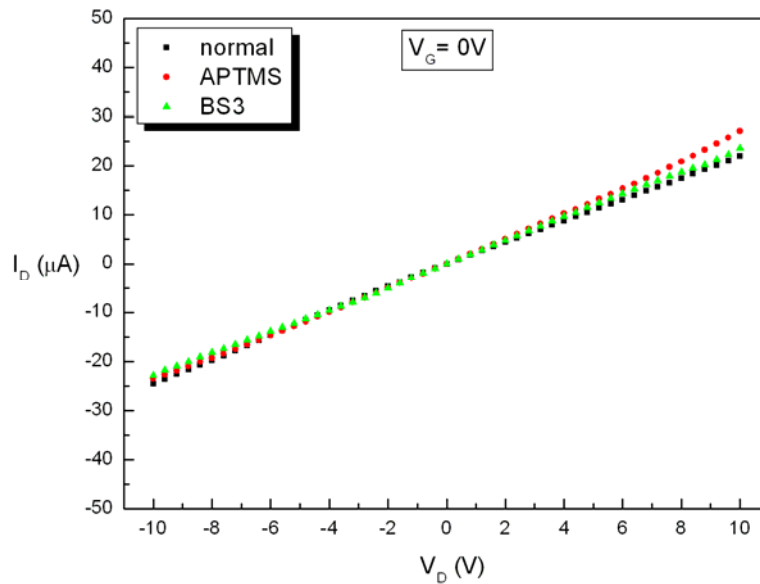
Figure 3-34. After the oxidation of 2min at 950℃, I_D-V_D curve of N-type

$Si_{0.89}Ge_{0.11}$ nanowire. The length of nanowire is 13 μ m.
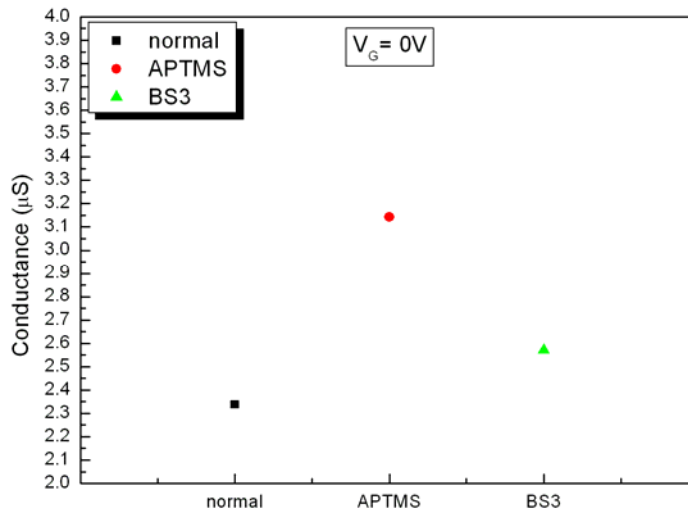
Figure 3-35. After the oxidation of 2min at 950℃, the conductance of N-type $Si_{0.93}Ge_{0.07}$ nanowire changes with different chemical molecules. The length of nanowire is 20 μm.
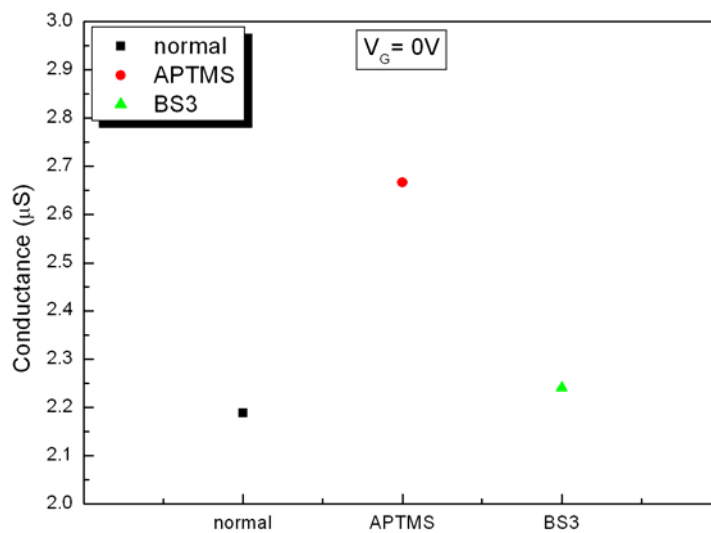
Figure 3-36. After the oxidation of 2min at 950℃, the conductance of N-type $Si_{0.89}Ge_{0.11}$ nanowire changes with different chemical molecules. The length of nanowire is 13 μm.
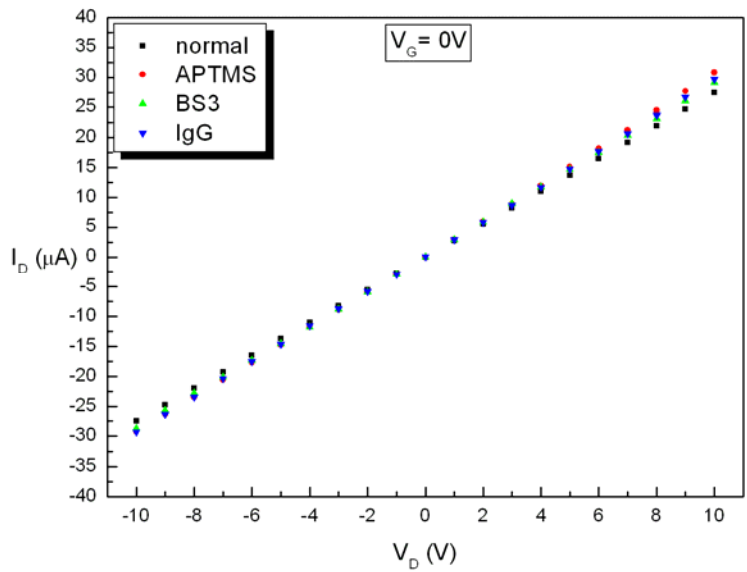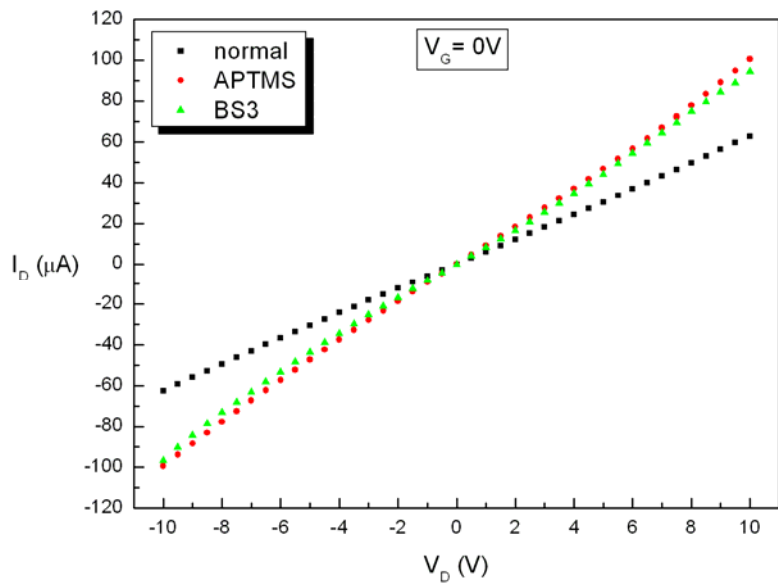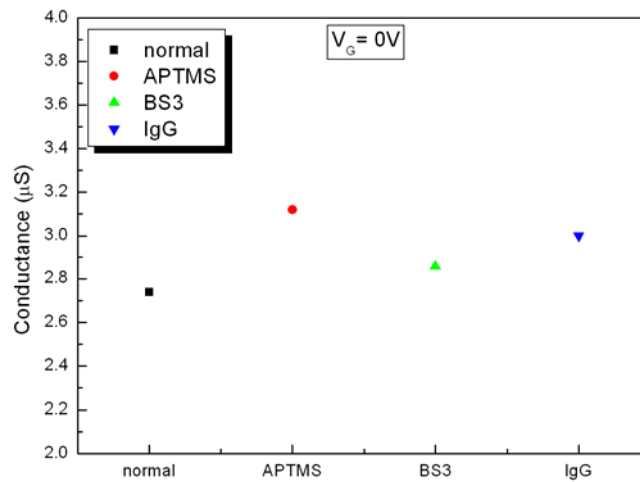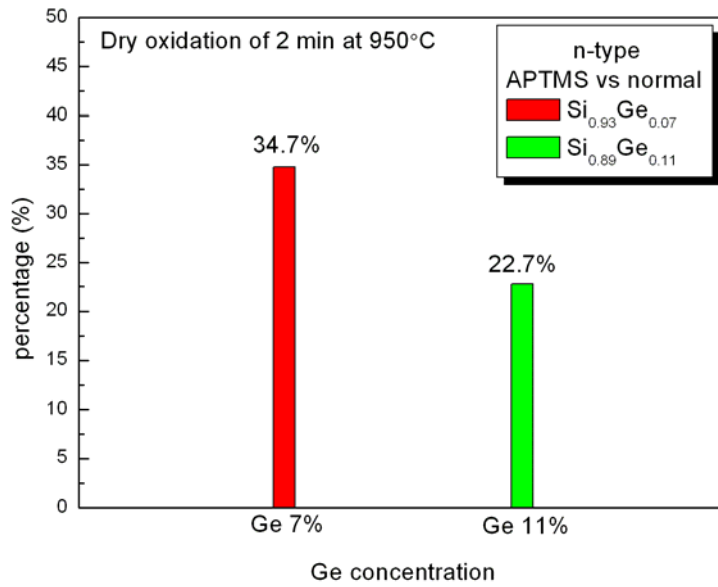
Figure 3-37. After the oxidation of 2min at 950℃, the sensitivity of SiGe

nanowires were enhanced.
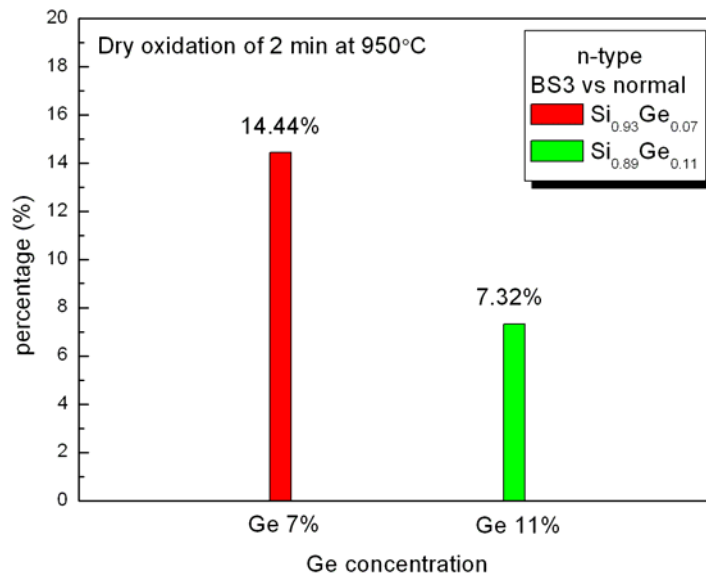
Figure 3-38. After the oxidation of 2min at 950℃, the sensitivity of SiGe

nanowires were enhanced.
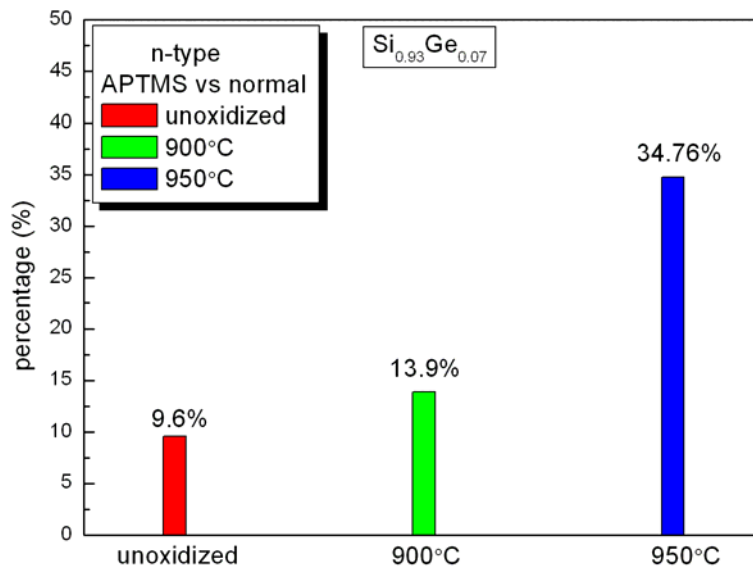
Figure 3-39. The sensitivity of $Si_{0.93}Ge_{0.07}$ nanowires were enhanced with different oxidation temperature.
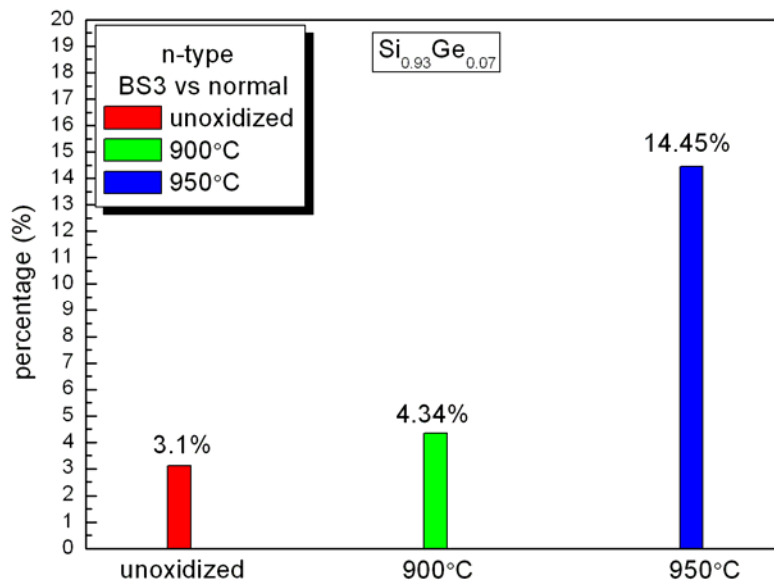
Figure 3-40. The sensitivity of $Si_{0.93}Ge_{0.07}$ nanowires were enhanced with different oxidation temperature.
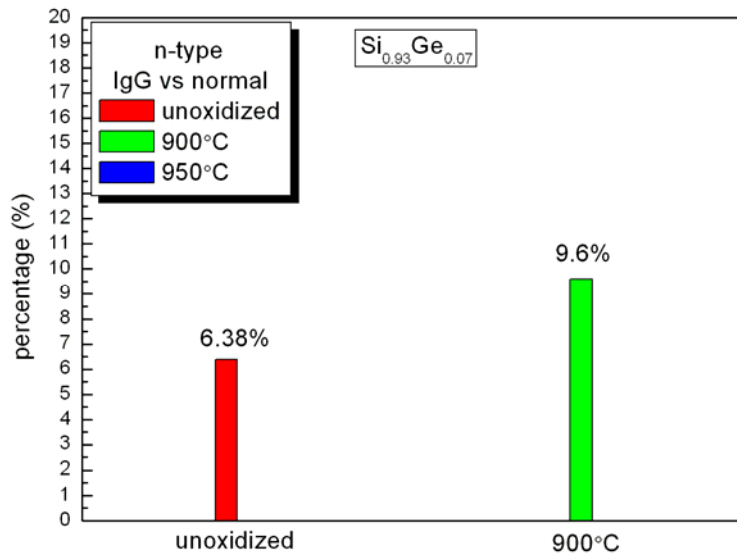
Figure 3-41. The sensitivity of $Si_{0.93}Ge_{0.07}$ nanowires were enhanced with different oxidation temperature.
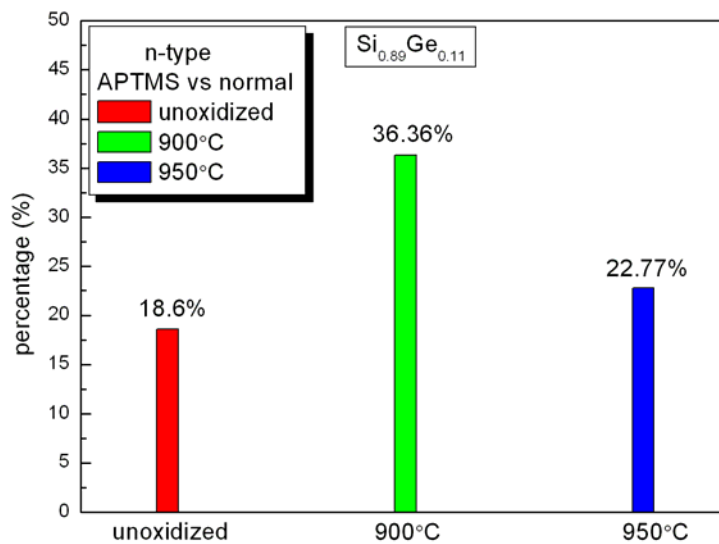
Figure 3-42. The sensitivity of $Si_{0.89}Ge_{0.11}$ nanowires changed with different temperature.
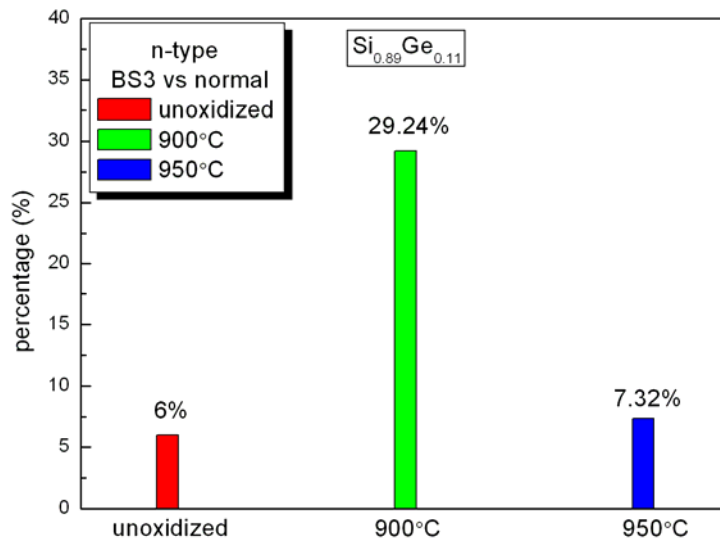
Figure 3-43. The sensitivity of $Si_{0.89}Ge_{0.11}$ nanowires changed with different temperature.

Reference:

[1] Yi Cui, Qingqiao Wei, Hongkun Park, and Charles M. Lieber, "Nanowire Nanosensors for Highly Sensitive and Selective Detection of Biological and Chemical Species", *Science*, Vol. 293, 1289, (2001)

[2] Hyunjin Lee, Seong-Wan Ryu, Jin-Woo Han, Lee-Eun Yu, Maesoon Im, Chungjin Kim, Sungho Kim, Eujung Lee, Kuk-Hwan Kim, Ju-Hyun Kim, Dong-il Bae, Sang-Cheol Jeon, Kwang Hee Kim, Gi Sung Lee, Jae Sub Oh, Yun Chang Park, Woo Bo Bae, Jung Jae Yoo, Jun Mo Yang, Hee Mok Lee, and Yang-Kyu Choi, "A Nanowire Transistor for High Performance Logic and Terabit Non-Volatile Memory Devices", *Symposium on VLSI Technology Digest of Technical Papers,* 144-145, (2007)

[3] G. Brambilla, F. Xu, and X. Feng, "Fabrication of optical fibre nanowires and their optical and mechanical characterization", *ELECTRONICS LETTERS,* Vol 42, 8, (2006)

[4] Shih-Ching Chen, Ting-Chang Chang, Po-Tsun Liu, Yung-Chun Wu, Po-Shun Lin, Bae-Heng Tseng, Jang-Hung Shy, S. M. Sze, Chun-Yen Chang, and Chen-Hsin Lien, "A Novel Nanowire channel Poly-Si TFT Functioning as Transistor and Nonvolatile SONOS Memory", *IEEE ELECTRON DEVICE LETTERS*, Vol. 28, 9, (2007)

[5] Q. Gao, Y. Kim, H. J. Joyce, P. Lever, S. Mokkapati, M. Buda, H. H. Tan and C. Jagadish, "Quantum Dots and Nanowires for Optoelectronic Device Application", *International Conference on Transparent Optical Networks,* Vol. 2, 242, (2006)

[6] Kook-Nyung Lee, Suk-Won Jung, Won-Hyo Kim, Min-Ho Lee,

Woo-Kyeong Seong, Mira Kim, and Yoon-Sik Lee, "Fabrication of silicon Nanowire for Biosensor Application", *IEEE SENSORS,* Vol. , 1269, (2006)

[7] Ajay Agarwal, I. K. Lao, K. Buddhharaju, N. Singh, N. Balasubramanian and D. L. Kwong, "Silicon Nanowire Array Bio-sensor Using Top-down CMOS Technology", *The 14th International Conference on Solid-State Sensors*, (2007)

[8] Inkyu Park, Zhiyong Li, and Albert P. Pisano, "Selective Functionalization of Silicon Micro/Nanowire Sensors via Localized Joule Heating", *Proceeding of the 2nd IEEE International Conference on Nano/Micro Engineered and Molecular Systems,* (2007)

[9] Z. Gao, A. Agarwal, A. D. Trigg, N. Singh, C. Fang, C. H. Tung and K. D. Buddharaju, "Silicon Nanowire Arrays For Ultrasensitive Label –free Detection of DNA", *The 14th International Conference on Solid-State Sensor*, (2007)

[10] Z. Li, Y. Chen, X. Li, T. I. Kamins, K. Nauka and R. S. Williams, "Sequence- Specific Label-Free DNA Sensors Based on Silicon Nanowires ", *Nano Letters*, Vol. 4, 245, (2004)

[11] Fernando Patolsky, Gengfeng Zheng, Oliver Hayden, Melike Lakadamyali, Xiaowei Zhuang and Charles M. Lieber, "Electrical detection of single viruses", *Proceeding of the National Academy Sciences of the U.S.A.*, Vol. 101, 14017, (2004)

[12] Zhlyong Fan, Deepanshu Dutta, Chung-Jen Chien, Hsiang-Yu Chen, Evan C. Brown, Pai-Chun Chang, and Jia G. Lu, "Electrical and photoconductive properties of vertical ZnO nanowires in high density arrays", *Applied Physics Letters*, Vol. 89, 2131110, (2007)

[13] E. Comini, G. Faglia, G. Sberveglien, Zhengwei Pan and Zhong L. Wang, "Stable and highly sensitive gas sensors based on semiconducting oxide nanobelts", *Applied Physics Letters*, Vol. 81, 10, (2002)

[14] Chao Li, Daihua Zhang, Xiaolei Liu, Song Han, Tao Tang, Jie Han, and Chongwu Zhou, "In_2O_3 nanowires as chemical sensors", *Applied Physics Letters*, Vol. 82, 10, (2003)

[15] Andrea Ponzoni, Elisabetta Comini, Giorgio Sberveglieri, Jun Zhou, Shao Zhi Deng, Ning Sheng Xu, Yong Ding, and Zhong Lin Wang, "Ultrasenstive and highly selective gas sensors using three-dimensional tungsten oxide nanowire networks", *Applied Physics Letters*, Vol. 88, 203101, (2006)

[16] Haiqing Liu, Jun Kameoka, David A. Czaplewski, and H. G. Craighead, "Polymeric Nanowire Chemical Sensor", *Nano Letters*, Vol. 4, 671, (2004)

[17] Yufeng Ma, Jianming Zhang, Guojin Zhang, and Huixin He, "Polyaniline Nanowires on Si Surfaces Fabricated with DNA Templates", *American Chemical Society,* Vol. 126, 7097, (2004)

[18] Kyun Tae Kim, Sang Jun Sim, and Sung Min Cho, "Hydrogen Gas Sensor Using Pd Nanowires Electro-Deposited Into Anodized Alumina Template", *IEEE Sensors Journal,* Vol. 6, 509, (2006)

[19] Frederic Favier, Erich C. Walter, MichealP. Zach, Thorsten Benter, and Reginald M. Penner, "Hydrogen Sensors and Switches from Electrodeposited Palladium Mesowire Arrays", *Science*, Vol. 293, 2227, (2001)

[20] Woong-Ki Hong, Dae-Kue Hwang, Il-Kyu Park, Gunho Jo,

Sunghoon Song, Seong-Ju Park, and Takhee Lee, "Realization of highly reproducible ZnO nanowire field effect transistor with n-channel depletion and enhancement modes", *Applied Physics Letters*, Vol. 90, 243103, (2007)

[21] Deli Wang, Yi Cui, Marc W. Bockrath, and Charles M. Lieber, "Nanowire Crossbar Arrays as Address Decoders for Integrated Nanosystems, Zhaohui Zhong", *Science*, Vol. 302, 1377, (2003)

[22] Duan, X.; Huang, Y.; Lieber, C. M., "Nonvolatile Memory and Programmable Logic from Molecule- Gated Nanowires", *Nano Letters*, Vol. 2, 487, (2002)

[23] Zhong, Z.; Qian, F.; Wang, D.; Lieber, C. M. , "Synthesis of p-Type Gallium Nitride Nanowires for Electronic and Photonic Nanodevices", *Nano Letters*, Vol. 3, 343, (2003)

[24] Mark S. Gudiksen, Xiangfeng Duan, Yi Cui, and Charles M. Lieber, "Highly Polarized Photoluminescence and Photodetection from Single Indium Phosphide Nanowires, Jianfang Wang", *Science*, Vol. 293, 1455, (2001)

[25] Xiangfeng Duan, Yu Huang, Ritesh Agarwal, Charles M. Lieber, "Single-nanowire electrically driven lasers", *Nature*, Vol. 421, 241, (2003)

[26] H. H. Solak, D. He, W. Li, S. Singh- Gasson, and F. Cerrina, "Exposure of 38 nm period grating patterns with extreme ultraviolet interferometric lithography", *Applied Physics Letters*, Vol. 75, 2328, (1999)

[27] R. Nemutudi, N.J. Curson, N.J. Appleyard, D.A. Ritchie, G.A.C. Jones , "Modification of a shallow 2DEG by AFM lithography",

Microelectronic Engineering, Vol. 57, 967, (2001)

[28] X.-M. Yan, S. Kwon, A. M. Contreras, J. Bolor, and G. A. Somorjai, "Fabrication of Large Number Density Platinum Nanowire Arrays by Size Reduction Lithography and Nanoimprint Lithography", vol. 5, 4, (2005)

[29] Y. K. Choi, T. J. King, C. Hu , "A Spacer Patterning Technology for Nanoscale CMOS", *IEEE Transactions on Electron Devices*, Vol. 49, 436, (2002).

[30] Paritosh Mohanty, Isun Yoon, Teajoon Kang, Kwanyong Seo, Kumar S. K. Varadwaj, Wonjun Choi, Q-Han Park, Jae Pyung Ahn, Yung Doug Suh, Hyotcherl Ihee, and Bongsoo Kim, "Simple Vapor-Phase Synthesis of Single-Crystalline Ag Nanowires and Single-Nanowire Surface-Enhanced Raman Scattering", *Journal American Chemical Society*, Vol. 129, 9576, (2007)

[31] Chao Li, Daihua Zhang, Song Han, Xiaolei Liu, Tao Tang, and Chonggwu Zhou, "Diameter-Controlled Growth of Single- Crystalline In$_2$O$_3$ Nanowires and Their Electronic Properties", *Advance Materials,* Vol. 15, 143, (2003)

[32] Adam P. Robinson, Gavin Bumell, Mingzhe Hu, and Judith L. MacManus-Driscoll, "Controlled, perfect ordering in ultrathin anodic aluminum oxide templates on silicon", *Applied Physics Letters*, Vol. 91, 143123, (2007)

[33] Yee-Chia Yeo, Qiang Lu, Tsu-Jae King, Chenming Hu, Takayuki Kawashima, Masato Oishi, Supika Mashiro, and Junro Sakai, "Enhanced Performance in Sub-100 nm CMOSFETs using Strained Epitaxial Silicon-Germanium", *IEDM,* 753, (2000)

[34] "The Ge enhance the sensitivity for bio-sensor", *IEEE International Nanoelectronics Conference,* (2008)

[35] J. Eugene, F. K. LeGoues, V. P. Kesan, S. S. lyer, and F. M. d'Heurle, "Diffusion versus oxidation rates in silicon-germanium alloys", *Applied Physics Letters*, Vol. 59, 1, (1991)

[36] H. K. Liou, P. Mei, U. Gennser, and E. S. Yang, "Effects of Ge concentration on SiGe oxidation behavior", *Applied Physics Letters*, Vol. 59, 10, (1991)

[37] F. K. LeGoues, R. Rosenberg, and B. S. Meyerson, "Kinetics and mechanism of oxidation of SiGe: dry versus wet oxidation", *Applied Physics Letters*, Vol. 54, 7, (1989)

[38] H. Tsutsu, W. J. Edwards, and D. G. Ast, "Oxidation of polycrystalline-SiGe alloys", *Applied Physics Letters*, Vol. 63, 3, (1994)

[39] Carl Wagner, "Formation ofComposite Scales Consisting of Oxides of Different Metals", *JOURNAL OF THE ELECTROCHEMICAL SOCIETY,* Vol. 99, 369, (1952)

[40] Carl Wagner, "Theoretical Analysis of the Diffusion Processes Determining the Oxidation Rate of Alloys", *JOURNAL OF THE ELECTROCHEMICAL SOCIETY,* Vol. 103, 627, (1956)

[41] T. Tezuka, N. Sugiyama, and S. Takagi, "Fabrication of strained Si on an ultrathin SiGe-on-insulator virtual substrate with a high-Ge fraction", *Applied Physics Letters*, Vol. 79, 1789, (2001)

[42] N. Sugiyama, T. Tezuka, T. Mizuno, M. Suzuki, Y. Ishikawa, N. Shibata, and S. Takagi, "Temperature effects on Ge condensation by thermal oxidation of SiGe-on-insulator structures", *Journal of Applied*

Physics, Vol. 95, 8, (2004)

[43] S. Balakumar, Suo Peng, K. M. Hoe, A. Agarwal, G. Q. Lo, R. Kumar, N. Balasubramanian, and D. L. Kwong, "SiGeO layer formation mechanism at the SiGe/oxide interface during Ge condensation", *Applied Physics Letters*, Vol. 90, 32111, (2007)

[44] Shu Nakaharai, Tsutormu Tezuka, Naoharu Sugiyama, Yoshihiko Moriyama, and Shin-ichi Takagi, "Characterization of 7-nm-thick strained Ge-on-insulator layer fabricated by Ge-condensation technique", *Applied Physics Letters*, Vol. 83, 17, (2003)

[45] S. Nakaharai, T. Tezuka, N. Hirashita, E. Toyoda, Y. Moriyama, N. Sugiyama, and S. Takagi, "Generation of Crystal Defects in Ge-on-Insulator (GOI) Layers in Ge-condensation Process", *The Third International SiGe Technology and Device Meeting (ISTDM),* (2006)

[46] B. Vincent, J. F. Damiencourt, V. Delaye, R. Gassilloud, L. Clavelier, and Y. Morand, "Stacking fault generation during relaxation of silicon germanium on insulator layers obtained by the Ge condensation technique", *Applied Physics Letters*, Vol. 90, 074101, (2007)

[47] Tsutomu Tezuka, Naoharu Sugiyama, Tomohisa Mizuno, and Shin-ichi Takagi, "Ultrathin Body SiGe-on-Insulator pMOSFETs With High-Mobility SiGeSurface Channels", *IEEE TRANSACTION ON ELECTRON DEVICES*, Vol. 50, 5, (2003)

[48] M, Spadafora, G. Privitera, A. Terrasi, S. Scalese, C. Bongiormo, A. Carnera, M. Di Marino, and E. Napolitani, "Oxidation rate enhancement of SiGe epitaxial films oxidized in dry ambient", *Applied Physics Letters*, Vol. 83, 18, (2003)

簡歷

姓　　名: 趙文全

性　　別: 男

出生日期: 民國 68 年 12 月 19 日

出　生　地: 台灣省新竹市

地　　址: 新竹市東大路三段 77 巷 34 號

學　　歷: 私立中華大學電機系　　(民國 88 年 9 月~民國 92 年 6 月)

　　　　　國立交通大學微電子奈米科技產業研發碩士班　　(民國

　　　95 年 2 月~民國 97 年 2 月)